

A TOPOLOGICAL MODEL FOR THE HOMFLY-PT POLYNOMIAL

CRISTINA ANA-MARIA ANGHEL AND CHRISTINE RUEY SHAN LEE

ABSTRACT. We give the first known topological model for the HOMFLY-PT polynomial. More precisely, we prove that this invariant is given by a set of graded intersections between explicit Lagrangian submanifolds in a *fixed configuration space* on a *Heegaard surface* for the link exterior. The submanifolds are supported on arcs and ovals on the surface.

The construction also leads to a topological model for the Jones polynomial constructed from Heegaard surfaces associated *directly to the link diagram*. In particular, it *does not rely* on a choice of a *braid representative* for the link. This opens up new avenues for investigation of the geometry of these invariants, as well as categorifications of geometric nature.

CONTENTS

1. Introduction	1
2. A local system	7
3. Twisted homology groups	12
4. Recovering the Jones polynomial	20
5. Recovering the HOMFLY-PT polynomial	31
References	46

1. INTRODUCTION

Since the celebrated discovery of the Jones polynomial, understanding the geometric and topological information encoded in related polynomial link invariants has been a central goal of quantum topology. Towards this goal, our aim is to realize these invariants as graded intersection pairings in coverings of configuration spaces to approach a purely geometrical description. We refer to such a description as a *topological model* for the invariant.

Main Results. In this paper, we provide the first topological model for the HOMFLY-PT polynomial $P_L(a, z)$, which is a 2-variable generalization of the Alexander polynomial $\Delta_L(t)$ and the Jones polynomial $J_L(q)$.

Let L be a link and D a diagram for L . Our topological models are based on a fixed configuration space of a punctured Heegaard surface associated to D . The number punctures on the surface and the number of particles in

the configuration space is fixed, depending just on the number of crossings of the diagram.

Theorem 1 (Topological model for the HOMFLY-PT polynomial via ovals). *Let $\Theta_H(D) \in \mathbb{Z}[a^{\pm 1}, z^{\pm 1}]$ be the state sum of graded intersections between explicit Lagrangian submanifolds in a fixed configuration space on the Heegaard surface, as in Definition 1.5. Then this topological model recovers the HOMFLY-PT invariant:*

$$\Theta_H(D) = P_L(a, z)$$

This provides a new topological perspective for the HOMFLY-PT invariant of a link, showing that it is encoded by the set of intersections between Lagrangian submanifolds in a configuration space on a Heegaard surface. These Lagrangian submanifolds are based on collections of ovals and arcs in the surface.

The function Θ_H gives a geometric interpretation to a state sum formulation of the HOMFLY-PT polynomial. We construct as well a new topological model of the (un-normalised) Jones polynomial $J_L(q)$ that recovers the Kauffman bracket.

Theorem 2 (Topological model for the Jones polynomial from link diagrams).

Let $\Theta_J(D) \in \mathbb{Z}[q^{\pm}]$ be the state sum of graded intersections in the same configuration space on our fixed Heegaard surface, as defined in Definition 1.4. Then it provides a topological model for the Jones polynomial, relying just on the choice of diagram D :

$$\Theta_J(D) = J_L(q).$$

We discuss how our results compare to known topological models for related quantum invariants.

Topological models of quantum invariants from braid representatives. In [13], Lawrence constructed a sequence of representations of braid groups on the homology of certain coverings of configuration spaces. Based on her work, Bigelow constructed a homological model for the Jones polynomial [6]. This area was further developed by the first author who obtained topological models for new families of quantum invariants such as colored Jones polynomials, colored Alexander polynomials, and the Witten-Reshetikhin-Turaev invariants [1, 3, 4].

Since HOMFLY-PT is not a quantum invariant in the sense that its representation-theoretic origins are less well understood, the existence of a topological model remains an open question. In this direction, Bigelow constructed a homological model for the A_N polynomials [7], which are specializations in one variable of the 2-variable HOMFLY-PT polynomial.

Topological models from link diagrams and Heegaard surfaces. All these topological models for quantum invariants rely on a choice of a braid representative for a link. Having in mind the open problem concerning the geometric information encoded by Jones and HOMFLY-PT polynomials we summarize two problems that we answer with Theorem 1 and Theorem 2.

Question 1. *Construct a topological model for the HOMFLY-PT polynomial.*

As far as the authors know, up to this moment no such model is known. In **Theorem 1** we prove that the HOMFLY-PT polynomial can be read off from a set of Lagrangian intersections in a fixed configuration space on a Heegaard surface Σ . These Lagrangians are based on sets of arcs and ovals in Σ .

Question 2. *Define a topological model for the Jones polynomial that does not depend on choosing a braid representative for the link.*

Theorem 2 provides the first topological model for the Jones polynomial from graded intersections in a configuration space on the Heegaard surface Σ . The model only depends on the link diagram and does not require a choice of braid representative.

Configuration space of a Heegaard Surface. We start with a diagram D for our link and consider a Heegaard surface Σ associated to it, which is in the exterior of our link. Our main topological tools are built up using graded intersections between Lagrangian submanifolds in the configuration space on a punctured version of Σ . Our main results show that we can obtain the Jones polynomial and HOMFLY-PT polynomial from an explicit set of graded Lagrangian intersections in a fixed configuration space on the surface. Let us make this precise.

Let n be the number of crossings of the link diagram D . First we fix a set of 8 punctures on Σ associated to each crossing (as in Figure 4) and an additional fixed point and consider Σ' to be the resulting Heegaard surface with $8n + 1$ punctures. We will be working on the configuration space of $2n$ particles on the punctured surface Σ' :

$$Conf_{2n}(\Sigma').$$

1.1. Generic Local system and homology groups. We define a local system on this configuration space:

$$(1) \quad \Phi : \pi_1(C_{2n}(\Sigma')) \rightarrow \mathbb{Z}^{8n} \\ \langle \{x_j\}_{j \in \{1, \dots, 8n\}} \rangle$$

After that, we consider the covering of the configuration space $C_{2n}(\Sigma')$ associated to this local system. Our tools are the middle dimension homology groups of this covering: the Borel-Moore homology \mathcal{H}_{2n}^{lf} and homology \mathcal{H}_{2n} ,

which are $\mathbb{Z}[x_1^{\pm 1}, \dots, x_{8n}^{\pm 1}]$ -modules (as defined in Definition 3.4). These homologies are related by a Poincaré-type duality:

$$\langle\langle \cdot, \cdot \rangle\rangle: \mathcal{H}_{2n}^{lf} \otimes \mathcal{H}_{2n} \rightarrow \mathbb{Z}[x_1^{\pm 1}, \dots, x_{8n}^{\pm 1}] \quad (\text{Proposition 3.5}).$$

We use homology classes that are given by lifts of Lagrangian submanifolds from the base space. The recipe for constructing such submanifolds is to fix a collection of $2n$ arcs (or circles) on the punctured Heegaard surface Σ' , consider their products and quotient to the unordered configuration space. We call such a set of curves the “geometric support” for our submanifold. Then our pairing can be read off from the base space: it is parametrized by intersection points between the geometric supports and graded by the local system.

Both topological models are constructed based on the same underlying topological data:

- the configuration space of $2n$ particles on the fixed punctured Heegaard surface Σ' : $C_{2n}(\Sigma')$
- the intersection pairing between homologies of its fixed \mathbb{Z}^{8n} covering space from above.

The difference is reflected in the choice of homology classes and specialization of coefficients, as follows.

1.2. Homology classes associated to a state. For the Jones polynomial, our idea is to fix a resolution associated to a Kauffman state and to “push it” on the surface. Then, we transform it into two collections of arcs and ovals.

For the HOMFLY-PT invariant there is an extra subtle idea. On the combinatorial side, we develop a state formula using descending diagrams and renormalized Kauffman states. Geometrically we encode this renormalization procedure by cutting a component. We do this by fixing a cutting point on the diagram and once we consider a state, we define the set of arcs and ovals by the same technique as for the Jones polynomial, but we shrink the oval associated to this cutting point. More precisely, we have the following cases.

1.2.1. Context for the Jones polynomial. Let σ be a Kauffman state. We define two sets of curves on Σ' : $F(\sigma)$ (given by arcs between the punctures) and $L(\sigma)$ (given by ovals around punctures). Then, as above, they lead to two homology classes (as in Definition 4.5):

$$\mathcal{F}(\sigma) \in \mathcal{H}_{2n}^{lf} \quad \text{and} \quad \mathcal{L}(\sigma) \in \mathcal{H}_{2n} \quad (\text{Figure 10}).$$

1.2.2. Context for the HOMFLY-PT polynomial. For this model we fix a point on our diagram and call it a “cutting point”. Then, once we have a renormalized Kauffman state σ_H , we associate another two sets of curves $F(\sigma_H)$ (given by arcs between the punctures) and $L(\sigma_H)$ (given by ovals

around punctures), but where we shrink the oval around the cutting point, as in Figure 17. They lead to the classes:

$$\mathcal{F}^H(\sigma_H) \in \mathcal{H}_{2n}^{lf} \quad \text{and} \quad \mathcal{L}^H(\sigma_H) \in \mathcal{H}_{2n} \quad (\text{Figure 17}).$$

1.3. Specialization associated to a state. We remark that the above homology classes depend on the choice of state, but they belong to the generic homology groups of the covering, which are intrinsic and do not depend on the state. Now, we define a specialization of coefficients associated to a fixed state, as in Definition 3.19.

Definition 1.1 (Change of coefficients for a state).

Consider $\alpha_Q^\sigma : \mathbb{Z}[x_1^{\pm 1}, \dots, x_{8n}^{\pm 1}] \rightarrow \mathbb{Z}[Q^{\pm 1}]$, which is constructed in a geometric manner such that it satisfies a certain *Monodromy Requirement* related to evaluations around the punctures from the surface (Definition 3.17).

Both models are then given by the generic intersection pairing \ll , \gg , between the classes associated to the state σ but specialized through α_Q^σ , for two different choices of Q .

Definition 1.2 (Specialization of coefficients for the Jones polynomial).

For a particular choice of $Q = Q_J$, we have the induced specialization $\alpha_J^\sigma : \mathbb{Z}[x_1^{\pm 1}, \dots, x_{8n}^{\pm 1}] \rightarrow \mathbb{Z}[q^{\pm 1}](1 - q - q^{-1})$ and the specialized intersection pairing as below (see Definition 3.22):

$$\ll , \gg_{\alpha_J^\sigma} : \mathcal{H}_{2n}^{lf} |_J \otimes \mathcal{H}_{2n} |_J \rightarrow \mathbb{Z}[q^{\pm 1}](1 - q - q^{-1}).$$

Definition 1.3 (Specialization for the HOMFLY-PT polynomial). For the case of the HOMFLY-PT polynomial we will use the change of coefficients $\alpha_H^\sigma : \mathbb{Z}[x_1^{\pm 1}, \dots, x_{8n}^{\pm 1}] \rightarrow \mathbb{Z}[a^{\pm 1}, z^{\pm 1}](1 - \frac{a-a^{-1}}{z})$ and the specialized groups (see Definition 3.23):

$$\ll , \gg_{\alpha_H^\sigma} : \mathcal{H}_{2n}^{lf} |_H \otimes \mathcal{H}_{2n} |_H \rightarrow \mathbb{Z}[a^{\pm 1}, z^{\pm 1}](1 - \frac{a - a^{-1}}{z}).$$

1.4. Topological formula for the Jones polynomial. We consider the state sum of such graded intersections between $\mathcal{F}(\sigma)$ and $\mathcal{L}(\sigma)$ over all choices of Kauffman states σ , as follows.

Definition 1.4 (Intersection form for the Jones polynomial). Let us consider the function $\Theta_J(D)$ defined as follows (see Definition 4.11):

$$\Theta_J(D)(q) := \sum_{\sigma \text{ Kauffman state}} q^{\frac{-i(D_\sigma(\alpha), D) + 3w(D)}{2}} \ll \mathcal{F}(\sigma), \mathcal{L}(\sigma) \gg_{\alpha_J^\sigma}.$$

Then, in Theorem 1 we show that this topological model $\Theta_J(D)(q)$ gives exactly the Jones polynomial of the link.

1.5. Topological formula for the HOMFLY-PT polynomial. For the model for the HOMFLY-PT polynomial, we define a state sum of the intersection pairings between classes $\mathcal{F}(\sigma_H)$ and $\mathcal{L}(\sigma_H)$ over all choices of renormalized Kauffman state σ_H . A subtle procedure for this part concerns the construction of the set of renormalized Kauffman states σ_H , presented in Section 5.

Definition 1.5 (Intersection form for the HOMFLY-PT polynomial). Let us consider the function $\Theta_H(D)$ defined as follows (see Definition 5.13):

$$\Theta_H(D)(a, z) := \sum_{\sigma_H \text{ renormalized Kauffman state}} \text{sgn}(\sigma_H) a^{i^a(\sigma_H)} z^{i^z(\sigma_H)} \ll \mathcal{F}^H(\sigma_H), \mathcal{L}^H(\sigma_H) \gg_{\alpha_H^{\sigma_H}}$$

Remark 1.6 (Geometric perspective for the HOMFLY-PT polynomial). *Theorem 1 shows that the HOMFLY-PT polynomial of a link is given by the set of graded intersections between the homology classes associated to the set of states:*

$$P_L(a, z) \longleftrightarrow \left\{ \begin{array}{l} \text{graded intersections } \ll \mathcal{F}^H(\sigma_H), \mathcal{L}^H(\sigma_H) \gg \\ \text{in the configuration space of } 2n \text{ points} \\ \text{on the punctured Heegaard surface } \Sigma' \end{array} \right\}_{\sigma_H \text{ state.}}$$

Remark 1.7 (Model for Jones polynomial vs. HOMFLY-PT polynomial). *Our first intersection model $\Theta_J(D)(q)$ leads to the Jones polynomial and the second renormalized model $\Theta_H(D)(a, z)$ gives the HOMFLY-PT polynomial. This, in turn, leads to the Alexander polynomial and normalized Jones polynomial.*

Comparing the two models for the case of the Jones polynomial we see that in one case we obtain the un-normalized version (where we do not cut the strand) and in the other we obtain the normalized version, where we cut the strand.

1.6. Connection to representation theory. Philosophically we expect this to have a deeper meaning coming from representation theory. The fact that the HOMFLY-PT invariant contains the Alexander polynomial as a specialization means, from a quantum point of view, that it contains a non-semisimple invariant. Geometrically this non-semisimplicity is encoded in the procedure of cutting of the strand and shrinking one oval from our geometric support.

It might be interesting to study this phenomenon in a deeper way and its impact on connections between the topological model for the HOMFLY-PT polynomial that we develop and representation-theoretic information encoded by this invariant.

1.7. New geometrical perspectives and categorifications. From the topological model of the HOMFLY-PT polynomial, we can obtain a topological model of the Alexander polynomial by specializing the variables $a \mapsto 1$

and $z \mapsto t^{1/2} - t^{-1/2}$, and since the definition of the Heegaard surface Σ used in our construction closely follows [17], where Ozsváth-Szabó determine the knot Floer homology of alternating knots with their setup, it is natural to ask about the relationship between two topological models for the Alexander polynomial: our model, and the one from knot Floer homology. We plan to investigate this question in the future.

Organization. Since the state sum model of the Jones polynomial through the Kauffman bracket is well-known, our choice of exposition is to first describe the intersection pairing. The technical construction spans Sections 2 and 3. We develop the specialization of the intersection form needed for the Jones polynomial and for the HOMFLY-PT polynomial in Sections 3.2 and 3.3. Finally, we prove that Θ_J recovers the Jones polynomial through the Kauffman bracket state sum definition in Section 4.6. In Section 5, we show that the model extends to the HOMFLY-PT polynomial through a state sum model in an analogous way and prove Theorem 1 in Section 5.6.

2. A LOCAL SYSTEM

2.1. Punctures and base points on a Heegaard surface of a link diagram. As defined in [15], a *compression body* is a 3-manifold V obtained from a surface Σ cross an interval $[0, 1]$ by attaching a finite number of 2-handles and 3-handles to $\Sigma \times \{0\}$. The component $\Sigma \times \{1\}$ of the boundary will be denoted by $\partial_+ V$, and $\partial V \setminus \partial_+ V$ will be denoted by $\partial_- V$.

Let L be a link in S^3 . A (generalized) *Heegaard splitting* for a link exterior $E(L)$ is a decomposition $E(L) = V \cup_\Sigma W$, where V is a compression body with $\partial_+ V \simeq \Sigma$ and $\partial_- V = \partial N(L)$, and W is a handlebody. The surface Σ is called a *Heegaard surface* for the link L .

Let D be a diagram of a link L . We follow Ozsváth-Szabó [17] in the construction of a Heegaard surface Σ of the link L from D . To each crossing χ of the diagram we associate a 4-punctured sphere as a local piece of the Heegaard surface:

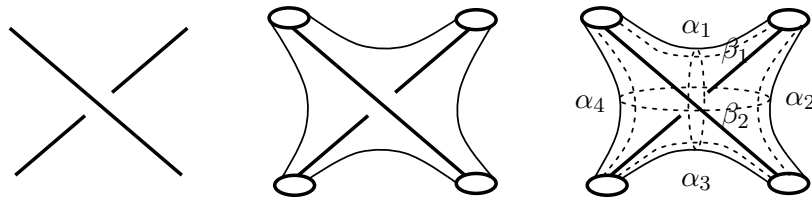


FIGURE 1. From left to right: a crossing, a 4-punctured sphere at a crossing, α and β curves.

To a crossing χ we also associate two beta curves $\beta_1(\chi), \beta_2(\chi)$, and four alpha arcs $\alpha_1(\chi), \alpha_2(\chi), \alpha_3(\chi), \alpha_4(\chi)$, corresponding to each quadrant of the crossing as also shown in Figure 1. Note the β curves are different from those

defined in [17]. Formally, each boundary circle is transverse to the projection plane and centered on the knot strand.

The surface Σ is built by identifying every pair of boundary circles on two 4-punctured spheres sharing the same knot strand, so that the α arcs are extended through each 4-punctured sphere, see Figure 2.

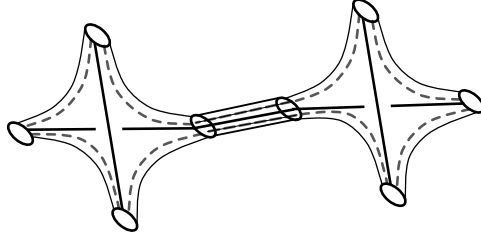


FIGURE 2. Gluing pieces of the Heegaard surface Σ along a knot strand.

We see the surface Σ is a Heegaard surface for $E(L)$ by thickening the surface to $\Sigma \times [0, 1]$, so that $\Sigma \times \{0\}$ contains the link L in its interior. At each crossing, add 2-handles to $\Sigma \times \{0\}$ to fill out the space between two strands of a crossing and $\Sigma \times \{0\}$. Finally, cap off the resulting sphere components with 3-handles.

By definition, the space $\Sigma \times [0, 1]$ with the 2- and 3-handles attached is a compression body V with $\partial_- V = \partial N(L)$. The complement of V in S^3 is bound by Σ and therefore a handlebody, and $V \cup_{\Sigma} (S^3 \setminus V)$ defines a Heegaard splitting of $E(L)$.

2.2. Intersection points. We will define the intersection pairing as arising from certain intersection points on the Heegaard surface Σ in the previous section.

Isotope the knot diagram so that every crossing is oriented with the North, South, East, and West quadrant between a pair of strands as on the left in Figure 3. First we define four points x_l, x_r, y_l, y_r on the surface at each crossing as indicated in the local picture:

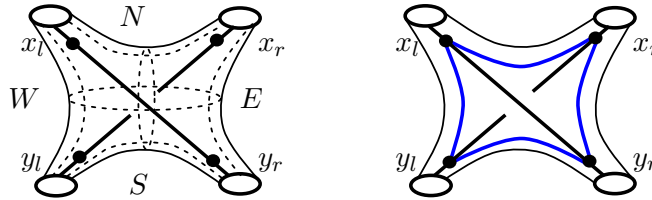


FIGURE 3. From left to right: four intersection points on Σ , blue colorings of the α -curves from resolutions.

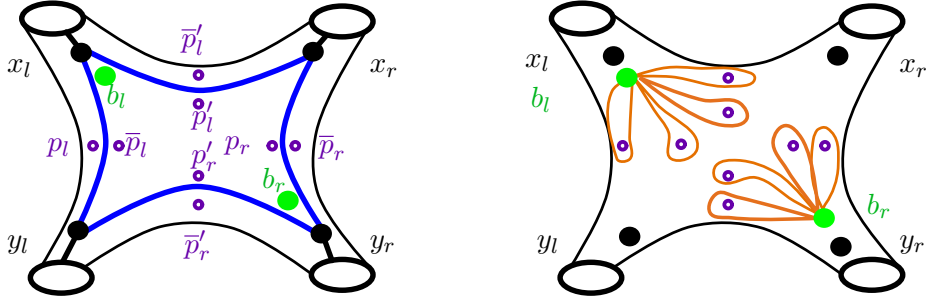


FIGURE 4. From left to right: A crossing and associated α arcs; additional purple punctures in relation to the arcs and base points; based orange loops γ_j encircling punctures.

Let n be the number of crossings in D . We mark additional points that avoid the α curves and the β curves and denote them by:

$$(2) \quad \begin{cases} p_l \text{ and } \bar{p}_l, \\ p_r \text{ and } \bar{p}_r, \\ p'_l \text{ and } \bar{p}'_l, \\ p'_r \text{ and } \bar{p}'_r, \end{cases} \text{ for } i \in \{1, \dots, n\} \text{ as in Figure 4.}$$

We choose an extra fixed point denoted by s on our surface that does not coincide with the above points.

2.3. Configuration space. We will be working in the configuration space of $2n$ particles on the surface Σ' obtained from Σ by removing the special puncture s and the sets of punctures and marked points:

$$\{p_l, \bar{p}_l, p_r, \bar{p}_r, p'_l, \bar{p}'_l, p'_r, \bar{p}'_r\} \text{ and } \{x_l, x_r, y_l, y_r\}$$

that are associated to all the crossings.

Next, for the grading procedure and the definition of the intersection pairing, we define a local system on this configuration space. For this purpose, we will need base points. Let us fix two base points at a crossing, as follows. We designate one puncture for each arc of an alpha curve at a crossing, obtaining two points: one inside the closed loop formed by connecting the α arc along each crossing, and the other is outside of the closed loop. We denote these points as in Figure 3:

$$(3) \quad \{\bar{b}_l, \bar{b}_r\} := \{x_l, y_r\}.$$

For a computational purpose, we choose two base points near the punctures \bar{b}_l, \bar{b}_r and we denote these points as:

$$(4) \quad \{b_l, b_r\}.$$

In addition we color the α arcs at a crossing blue. Extensions of α arcs between crossings will be colored black.

Definition 2.1. All of this discussion is for a fixed crossing. We have n crossings in our diagram, denoted c_1, \dots, c_n and for crossing c_i we add i as an index to the chosen points, as below:

$$(5) \quad c_i : \text{ Marked points } \{x_l^i, x_r^i, y_l^i, y_r^i\}$$

$$(6) \quad \text{Punctures } \{p_l^i, \bar{p}_l^i, p_r^i, \bar{p}_r^i, (p')_l^i, (\bar{p}')_l^i, (p')_r^i, (\bar{p}')_r^i\}$$

$$(7) \quad \text{Base points } \{b_l^i, b_r^i\} := \{x_l, y_r\}.$$

Definition 2.2 (Base points and intersection points). Let us define the set of all base points, associated as above to the set of crossings by:

$$\{b_1, \dots, b_{2n}\}.$$

Also we consider the set of all punctures on the surface and denote it as below:

$$\{p_1, \dots, p_{8n}, x_1, \dots, x_{4n}\}.$$

We remark that this means that our punctured surface Σ' is:

$$\Sigma' = \Sigma \setminus \{p_1, \dots, p_{8n}, x_1, \dots, x_{4n}, s\}.$$

Next, we define a local system on a specific configuration space on this punctured surface Σ' . For this, we will use a collection of loops that are based in $\{b_1, \dots, b_{2n}\}$ and go around the punctures $\{p_1, \dots, p_{8n}\}$, as follows.

Definition 2.3 (Loops around punctures). For a fixed $i \in \{1, \dots, n\}$ we look at the crossing c_i and consider a collection of eight curves which go around punctures, distributed as below:

- 4 loops based in b_l^i which go around the punctures $p_l^i, \bar{p}_l^i, (p')_l^i$ and $(\bar{p}')_l^i$
- 4 loops based in b_r^i which go around the punctures $p_r^i, (\bar{p})_r^i, (p')_r^i$ and $(\bar{p}')_r^i$, as in the last figure on the right of Figure 4.

We denote this set of curves by $\{\gamma_1^i, \dots, \gamma_8^i\}$.

Definition 2.4 (Set of loops). Further, we denote the set of all loops around punctures from above as:

$$\{\gamma_1, \dots, \gamma_{8n}\}.$$

For $j \in \{1, \dots, 2n\}$ define $\tau(j)$ to be the index of the base point within $\{b_1, b_2, \dots, b_{2n}\}$ that belongs to γ_j :

$$(8) \quad b_{\tau(j)} \in \gamma_j.$$

2.4. Local system. In this part we introduce a local system on our surface with punctures Σ' . Let $C_{2n}(\Sigma')$ be the unordered configuration space of $2n$ points on Σ' . More specifically, this is given by:

$$C_{2n}(\Sigma') := \{(z_1, \dots, z_{2n}) \in (\Sigma')^{\times 2n} \mid z_i \neq z_j, \forall 1 \leq i < j \leq 2n\} / Sym_{2n}$$

where Sym_{2n} is the symmetric group of order $2n$.

We fix a base point in this covering space, given by the collection of base points associated to all the crossings, denoted by:

$$(9) \quad \mathbf{d} := (b_1, \dots, b_{2n}) \in C_{2n}(\Sigma').$$

Definition 2.5. (Local system on $C_{2n}(\Sigma')$) Let us start with the abelianization map by

$$ab : \pi_1(C_{2n}(\Sigma')) \rightarrow H_1(C_{2n}(\Sigma')).$$

We remark that in this homology group we have $2n$ special homology classes, given by loops in the configuration space where we keep all particles fixed except one, which moves on a loop $\gamma_i(t)$.

More precisely, consider the set of loops from below.

Definition 2.6 (Loops in the configuration space). For a index $j \in \{1, \dots, 8n\}$ let us consider the following loops in $C_{2n}(\Sigma')$:

$$\gamma'_i(t) := \{(b_1, b_2, \dots, b_{\tau(j)-1}, \gamma_j(t), b_{\tau(j)+1}, \dots, b_{4n})\}, t \in [0, 1]$$

Lemma 2.7. *The homology classes of these curves*

$$\{[\gamma'_1], \dots, [\gamma'_{8n}]\}$$

form a linearly independent set in the homology of the configuration spaces $H_1(C_{2n}(\Sigma'))$.

Definition 2.8 (Subgroup in the homology group). Consider the subgroup generated by the classes of these elements:

$$H := \langle [\gamma'_1], \dots, [\gamma'_{4n}] \rangle \simeq \mathbb{Z}^{8n} \subset H_1(C_{2n}(\Sigma')).$$

Also, following Lemma 2.7 we have the isomorphism

$$\begin{aligned} \nu : H &\simeq \mathbb{Z}^{8n} \\ &\langle [\gamma'_j] \rangle \mapsto \langle x_j \rangle \end{aligned}$$

defined by the formula: $\nu([\gamma'_j]) = x_j, \forall j \in \{1, \dots, 8n\}$.

Definition 2.9 (Projection map). We have now the subgroup H in the homology group of the configuration space. Consider the associated projection map which we denote as below:

$$(10) \quad p : H_1(C_{2n}(\Sigma')) \rightarrow \mathbb{Z}^{8n}.$$

Definition 2.10. (Local system) We consider the local system given by the composition of the three morphisms defined above:

$$(11) \quad \begin{aligned} \Phi : \pi_1(C_{2n}(\Sigma')) &\rightarrow \mathbb{Z}^{8n} \\ &\langle \{x_j\}_{j \in \{1, \dots, 8n\}} \rangle \\ \Phi &= \nu \circ p \circ ab. \end{aligned}$$

Definition 2.11 (Covering space). Let $\tilde{C}_{2n}(\Sigma')$ be the covering of the configuration space associated to the local system Φ .

Definition 2.12 (Base point in the covering space). We also fix a base point in this covering space, denoted by $\tilde{\mathbf{d}}$, which belongs to the fiber over \mathbf{d} in $\tilde{C}_{2n}(\Sigma')$.

3. TWISTED HOMOLOGY GROUPS

We consider certain versions of the relative homology of the covering space $\tilde{C}_{2n}(\Sigma')$. More specifically, we will make use of a subspace of the Borel-Moore homology of the above covering space, coming from the Borel-Moore homology of the base space, twisted by the local system.

Definition 3.1. Let us consider two homology groups, as below:

- $H_n^{\text{lf}}(\tilde{C}_{2n}(\Sigma'), \mathbb{Z})$ the Borel-Moore homology of $\tilde{C}_{2n}(\Sigma')$.
- $H_n(\tilde{C}_{2n}(\Sigma'), \mathbb{Z})$ be the homology of our covering.

Remark 3.2. *There is a subtle difference between the Borel-Moore homology of a covering space and the twisted Borel-Moore homology of the base space. We will work with the homology of the covering space rather than the twisted homology of the base space.*

Proposition 3.3 ([5], Theorem E). *There are natural injective maps:*

$$(12) \quad \begin{aligned} \iota &: H_n^{\text{lf}}(C_{2n}(\Sigma'); \mathcal{L}_\Phi) \rightarrow H_n^{\text{lf}}(\tilde{C}_{2n}(\Sigma'), \mathbb{Z}) \\ \iota^\partial &: H_n(C_{2n}(\Sigma'); \mathcal{L}_\Phi) \rightarrow H_n(\tilde{C}_{2n}(\Sigma'), \mathbb{Z}). \end{aligned}$$

In the above equations \mathcal{L}_Φ is the rank 1 local system associated to Φ ([5, Definition 2.7]).

Definition 3.4 (Homology groups). We denote the above submodules in the homologies of the covering space (which are modules over $\mathbb{Z}[x_1^{\pm 1}, \dots, x_{8n}^{\pm 1}]$):

- $\mathcal{H}_{2n}^{\text{lf}} \subseteq H_n^{\text{lf}}(\tilde{C}_{2n}(\Sigma'), \mathbb{Z})$ and
- $\mathcal{H}_{2n} \subseteq H_n(\tilde{C}_{2n}(\Sigma'), \mathbb{Z})$.

The submodules $\mathcal{H}_{2n}^{\text{lf}}$ and \mathcal{H}_{2n} are given by the images of the homology with twisted coefficients in the homology of the covering space via the inclusions ι and ι^∂ respectively.

Using this notation, the homology groups of the covering become modules over

$$(13) \quad \mathbb{Z}[x_1^{\pm 1}, \dots, x_{8n}^{\pm 1}].$$

The description of these homology groups has certain subtleties, but for our purpose we will use very precise classes given by submanifolds in the configuration space on the punctured surface Σ' .

In what follows we describe a geometric intersection pairing between these homologies of the covering space with respect to different parts of its boundary. The existence of this pairing is a consequence of a Poincaré-Lefschetz duality for twisted homology [5, Proposition 3.2] together with a relative cap product for twisted homology as described in [5, Lemma 3.3]. These two maps induce an intersection pairing between homology groups, as in [5].

Proposition 3.5. ([5, Proposition 7.6]) *There exists a topological intersection pairing:*

$$\langle\langle \cdot, \cdot \rangle\rangle: \mathcal{H}_{2n}^{lf} \otimes \mathcal{H}_{2n} \rightarrow \mathbb{Z}[x_1^{\pm 1}, \dots, x_{8n}^{\pm 1}].$$

3.1. Computing the intersection pairing. We will need the precise form of this intersection pairing in the next part so we sketch the key components for its formula, which is presented in [5, Section 7]. Recall we are working with coefficients that belong to the group ring presented in (13). For this, we introduce the following notation.

Definition 3.6. Let $\tilde{\Phi}$ be the morphism induced by the local system Φ , which takes values in the group ring of \mathbb{Z}^{4n} :

$$(14) \quad \tilde{\Phi}: \pi_1(C_{2n}(\Sigma)) \rightarrow \mathbb{Z}[x_1^{\pm 1}, \dots, x_{8n}^{\pm 1}].$$

We use this morphism for the computation of the intersection pairing as follows. Fix two homology classes

$$H_1 \in \mathcal{H}_{2n}^{lf} \text{ and } H_2 \in \mathcal{H}_{2n}.$$

Suppose H_1 and H_2 are given by the lifts of two submanifolds $X_1, X_2 \subseteq C_{2n}(\Sigma)$, which we denote $\tilde{X}_1, \tilde{X}_2 \subseteq \tilde{C}_{2n}(\Sigma')$. We further assume that X_1 and X_2 intersect transversely in a finite number of points.

For an intersection point $x \in X_1 \cap X_2$ we construct a loop $l_x \subseteq C_{2n}(\Sigma')$.

Definition 3.7. Construction of the associated loop l_x

Suppose we have two paths $\gamma_{X_1}, \gamma_{X_2}$ starting in $\mathbf{d} = (b_1, \dots, b_{2n})$ and ending on X_1, X_2 respectively. Also, we assume that: $\tilde{\gamma}_{X_1}(1) \in \tilde{X}_1$ and $\tilde{\gamma}_{X_2}(1) \in \tilde{X}_2$. Choose also two paths $\delta_{X_1}, \delta_{X_2}: [0, 1] \rightarrow C_{2n}(\Sigma')$ such that:

$$(15) \quad \begin{cases} \text{Im}(\delta_{X_1}) \subseteq X_1; \delta_{X_1}(0) = \gamma_{X_1}(1); \delta_{X_1}(1) = x \\ \text{Im}(\delta_{X_2}) \subseteq X_2; \delta_{X_2}(0) = \gamma_{X_2}(1); \delta_{X_2}(1) = x. \end{cases}$$

The composition of these paths gives a loop, as follows:

$$l_x = \gamma_{X_1} \circ \delta_{X_1} \circ \delta_{X_2}^{-1} \circ \gamma_{X_2}^{-1}.$$

Denote by α_x the sign of the geometric intersection at the point x between X_1 and X_2 (in the base configuration space). See Figure 11 for an example of l_x .

Proposition 3.8 (Intersection pairing from intersections in the base space). *The intersection pairing can be described from the set of loops l_x and the local system as below:*

$$(16) \quad \ll H_1, H_2 \gg = \sum_{x \in X_1 \cap X_2} \alpha_x \cdot \Phi(l_x) \in \mathbb{Z}[x_1^{\pm 1}, \dots, x_{8n}^{\pm 1}].$$

3.2. Specialization of coefficients associated to a state. In the next few sections, we set up the specializations of coefficients for the intersection pairing \ll, \gg so that they correctly compute key quantities in the definition of the Jones polynomial through the state sum from the Kauffman bracket, and in the definition of the HOMFLY-PT polynomial through a similar state sum. We conclude Section 3 with explicit specializations of the intersection pairing for both polynomials in Section 3.3.

Coloring of Kauffman state circles. Fix a link diagram D . Our first task for constructing the specialization is to define a coloring on the state circles resulting from applying a Kauffman state D .

Definition 3.9. A *Kauffman state* $\sigma : c(D) \rightarrow \{\pm\}$ is a function on the set of crossings of D that assigns to a crossing \times the $+$ -resolution \smile (or the $-$ -resolution \frown).

Let σ be a Kauffman state on a link diagram D . Replacing each crossing of the diagram with the choice of the $+$ - or $-$ - resolution by the Kauffman state results in a set of disjoint circles S_σ . A circle in S_σ is called a *state circle*. We define a coloring on the set of state circles such that every state circle is bicolored with an even number of blue segments and the same number of black segments, and the coloring alternates between blue and black as we traverse each state circle:

At every crossing, color both types of arcs resulting from the choice of the resolution blue. This is shown in Figure 5.

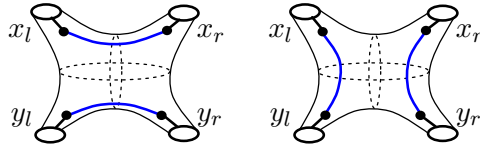


FIGURE 5. Colorings on the arcs of the resolution.

Keep the rest of the link strands black. Given a Kauffman state σ , replacing each crossing by the choice of the resolution by the state now results in a set of disjoint bi-colored circles.

Remark 3.10. *By construction, for each state σ there are twice as many blue-colored arcs as the number of crossings in the link diagram. Also, there are twice as many black-colored arcs as the number of crossings.*

This property comes from the fact that between an adjacent pair of blue colored arcs on the same strand there is a black arc. Therefore, there are also twice as many blue colored arcs as the number of crossings in the diagram. **Special punctures associated to a state.** Next we fix a Kauffman state σ . As we have seen, there is an associated set of disjoint circles on the surface, denoted by S_σ . Since our surface Σ is constructed from the knot diagram D in a plane π , we will fix a projection of the set of punctures onto π and denote this set as: $\{\tilde{p}_1, \dots, \tilde{p}_{8n}, x_1, \dots, x_{4n}, \tilde{s}\}$.

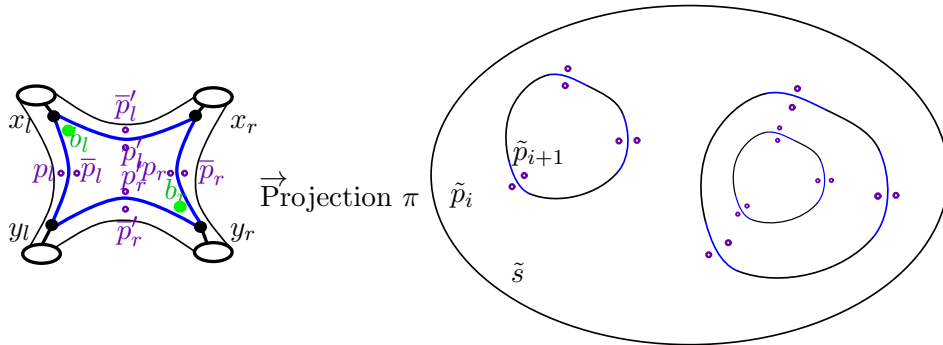


FIGURE 6. On the projection plane, the state circles may contain other circles.

Up to isotopy, we can assume that the state circles do not project onto the punctures. Denote by S'_σ the set of projections of the circles from S_σ . Without loss of generality, we can suppose that the puncture \tilde{s} “at infinity” does not belong to the disk bounded by any circle from S' in π .

We define the specialization of coefficients associated to the local system Φ using the above projections.

Definition 3.11 (Disks and punctures associated to state circles). Let C be a state circle from S and $C' \in S'$ its projection onto the plane of the knot diagram. We denote by D^C the disk bounded by C' in this plane, and called it the *state disk associated to C* .

Definition 3.12 (Punctures associated to state circles). Let C be a state circle and consider its associated state disk $D^C \subseteq \pi$. The disk D^C potentially contains some other disks associated to other state circles. We consider the region in the plane obtained from D^C by removing all these disks, and denote this region by R^C .

Lemma 3.13. *For any state circle C , the associated region R^C contains at least one puncture from the set $\{\tilde{p}_1, \dots, \tilde{p}_{8n}\}$.*

Proof. The state circle C is constructed from the blue-colored arcs associated to the resolution σ . Recall there are two punctures associated to each such arc, say p^j and \bar{p}^j , see Figure 4. Exactly one of these punctures projects

inside the disc D^C . Since these punctures are chosen in a tubular neighbourhood of the arc, they do not belong to any other associated discs that lie inside D^C . So, the projection of the puncture lies in the region R^C . \square

Definition 3.14 (σ -punctures). For a state circle $C_i \in S_\sigma$ choose one of the punctures guaranteed by the proof of Lemma 3.13 that projects inside R^C and denote it as P^i .

Also denote the evaluation of the local system Φ around this puncture by $x_{f(i)}$, where $f(i) \in \{1, \dots, 4n\}$.

Following the procedure described above, each circle in the collection of state circles $S_\sigma = \{C_1, \dots, C_{|\sigma|}\}$ has an associated puncture. We call this collection of “special punctures” associated to the state σ :

$$\{P^1, \dots, P^{|\sigma|}\} \subseteq \{\tilde{p}_1, \dots, \tilde{p}_{8n}\}$$

the set of σ -punctures.

Definition 3.15 (σ -punctures inside a fixed disk). For a circle $C_i \in S_\sigma$ consider all the σ -punctures associated to other state circles $C_{i'} \subset C_i$ that belong to the associated disk D^{C_i} that are not the chosen puncture P^i . Denote this set as below:

$$(17) \quad N^i := \{N_1^i, \dots, N_{\tau(i)}^i\} \subseteq \{P^1, \dots, P^{|\sigma|}\}.$$

Also denote the evaluation of the local system Φ around each of these punctures by $x_{g_i(j)}$, where $j \in \{1, \dots, \tau(i)\}$ and $g_i(j) \in \{1, \dots, 4n\}$.

Generic Specialization of coefficients. We define a specialization of coefficients for our local system, such that the monodromies that are “seen” through this specialization are just the ones around the set of σ -punctures. Recall that we have the local system introduced in Definition 3.6:

$$(18) \quad \tilde{\Phi} : \pi_1(C_{2n}(\Sigma)) \rightarrow \mathbb{Z}[x_1^{\pm 1}, \dots, x_{4n}^{\pm 1}].$$

Our aim is to introduce a change of coefficients that will lead to the desired intersection of homology classes, once specialized. We do this in two steps. First we project onto $\mathbb{Z}^{|\sigma|}$, which means that we count only the monodromies around σ -punctures. After that, we evaluate each component of $\mathbb{Z}^{|\sigma|}$ towards polynomials in one or two variables, associated to the case of the Jones polynomial or HOMFLY-PT polynomial, respectively. Let us make this precise.

Step 1-Mark the σ -punctures

Definition 3.16 (Projection map which keeps just the σ -punctures). Let us denote the following projection map

$$(19) \quad p : \quad \mathbb{Z}[x_1^{\pm 1}, \dots, x_{8n}^{\pm 1}] \quad \rightarrow \quad \mathbb{Z}[x_{f(1)}^{\pm 1}, \dots, x_{f(|\sigma|)}^{\pm 1}].$$

Step 2- Evaluate monodromies around σ -punctures

The second step prescribes the evaluation of monodromies around each σ -puncture such that a monodromy requirement is satisfied. The main idea is that when we count the contributions of the above evaluations around punctures belonging to any state disk we always obtain a fixed monomial.

This condition that we get a fixed monomial for each state circle will play a key role that ensures our intersection of homology classes gives the Kauffman bracket when evaluated on the set of state circles. We proceed as follows.

Definition 3.17 (Requirement for specialization of coefficients). Fix Q to be a polynomial or an indeterminate. We search for a change of coefficients:

$$(20) \quad \alpha_Q^\sigma : \mathbb{Z}[x_1^{\pm 1}, \dots, x_{8n}^{\pm 1}] \rightarrow \mathbb{Z}[Q^{\pm 1}],$$

which is a ring homomorphism and satisfies the following *Monodromy Requirement*.

Monodromy Requirement Consider a state circle C_i and the monodromies around punctures associated to the σ -punctures inside D^{C_i} . The requirement is that the product of all these monodromies gets evaluated through α_Q^σ to our fixed indeterminate Q .

Lemma 3.18. *There exists a change of coefficients α_Q^σ , which we construct explicitly and which satisfies the Monodromy Requirement.*

Proof. Since the Monodromy Requirement contains obstructions for evaluation of monodromies just around σ -punctures, it means that such α_Q^σ should factor through the projection p , so it is enough to define

$$(21) \quad \alpha_Q^\sigma : \mathbb{Z}[x_{f(1)}^{\pm 1}, \dots, x_{f(|\sigma|)}^{\pm 1}] \rightarrow \mathbb{Z}[Q^{\pm 1}].$$

We will proceed by an inductive argument. First, we look at state circles whose associated disks do not contain any other disk. If C_i is such a state circle, then D^{C_i} contains just a σ -puncture, namely P^i . In this case, we define:

$$(22) \quad \alpha_Q^\sigma(x_{f(i)}) = Q.$$

This means that the unique puncture associated to such a disk has the monodromy specialized to Q .

We proceed to define α_Q^σ on every $x_{f(i)}$ for which the corresponding special puncture P^i is contained in a state circle whose associated disk does not contain any other disk.

Inductively, consider a state circle C_i which contains other state circles, and suppose that we have defined the function α_Q^σ around all punctures associated to the region

$$D^{C_i} \setminus R^{C_i},$$

which are:

$$(23) \quad N^i = \{N_1^i, \dots, N_{\tau(i)}^i\} \subseteq \{P^1, \dots, P^k\},$$

and that α_Q^σ satisfies the Monodromy requirement for all the state circles $C' \subset D^{C_i}$. Recall that the local system Φ evaluates monodromies around these puncture, by:

$$x_{g_i(j)},$$

where $j \in \{1, \dots, \tau(i)\}$ and $g_i(j) \in \{1, \dots, 4n\}$, see Definition 3.15. This means that we have already defined :

$$\alpha_Q^\sigma(x_{g_i(j)}), \text{ for } j \in \{1, \dots, \tau(i)\}.$$

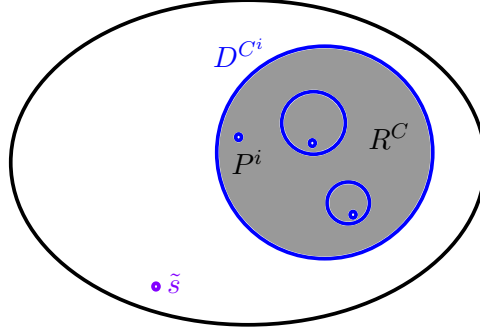


FIGURE 7. A fixed state circle C_i and its associated disk D^{C_i} with chosen puncture P^i and other punctures associated to other disks contained in D^{C_i} .

For the inductive case, we need only to figure out how α_Q^σ evaluates around the puncture P^i . We set the change of coefficients associated to the σ -puncture P^i as below:

$$(24) \quad \alpha_Q^\sigma(x_{f(i)}) = Q \cdot \prod_{j=1}^{\tau(i)} \alpha_Q(x_{g_i(j)})^{-1}.$$

With this definition, we see that the evaluation of α_Q^σ on variables on all punctures inside of the state disc D^{C_i} including P^i is precisely Q , which satisfies exactly the Monodromy Requirement for the state circle C_i . Following this procedure to define α_Q^σ for all the state circles in S_σ , we obtain the change-of-coefficients map α_Q^σ that satisfies the Monodromy Requirement for all state circles. Extending it by linearity to $\mathbb{Z}[x_1^{\pm 1}, \dots, x_{8n}^{\pm 1}]$, we obtain the desired function. \square

Definition 3.19 (Generic change of coefficients). Let us fix such a change of coefficients:

$$(25) \quad \alpha_Q^\sigma : \mathbb{Z}[x_1^{\pm 1}, \dots, x_{8n}^{\pm 1}] \rightarrow \mathbb{Z}[Q^{\pm 1}]$$

satisfies the conditions and *Monodromy Requirement* from Definition 3.17.

We recall that our homology groups of the covering space are modules over $\mathbb{Z}[x_1^{\pm 1}, \dots, x_{8n}^{\pm 1}]$ (as in (13)) and we have the associated intersection pairing

$$\langle\langle \cdot, \cdot \rangle\rangle_{\alpha_Q^\sigma}: \mathcal{H}_{2n}^{lf} \otimes \mathcal{H}_{2n} \rightarrow \mathbb{Z}[x_1^{\pm 1}, \dots, x_{8n}^{\pm 1}].$$

Definition 3.20 (Q -specialization of coefficients). We consider the specializations of these modules using the specialization of coefficients α_Q^σ :

$$\mathcal{H}_{2n}^{lf} |_{\alpha_Q^\sigma} \quad \text{and} \quad \mathcal{H}_{2n} |_{\alpha_Q^\sigma}.$$

Then, we have an associated specialized intersection pairing which we denote as below:

$$(26) \quad \langle\langle \cdot, \cdot \rangle\rangle_{\alpha_Q^\sigma}: \mathcal{H}_{2n}^{lf} |_{\alpha_Q^\sigma} \otimes \mathcal{H}_{2n} |_{\alpha_Q^\sigma} \rightarrow \mathbb{Z}[Q^{\pm 1}].$$

3.3. Specializations for the Jones and HOMFLY-PT polynomials.

We have seen that once we fix an indeterminate Q , we have a recipe to define a specialization of coefficients that satisfy the Monodromy Requirement, see Definition 3.20. Now we turn our attention to the invariants that we want to achieve, namely the Jones polynomial and the HOMFLY-PT polynomial, respectively. In this section, we introduce the specialization of coefficients that we will use for each of these cases. They will both be constructed as α_Q but the only difference is that we will use different indeterminates for the Jones polynomial case and for the HOMFLY-PT polynomial case, as follows.

Definition 3.21 (Fixing the specializations). Let us define two indeterminates as below:

- $Q_J := 1 - q - q^{-1}$ for the Jones polynomial
- $Q_H := 1 - \frac{a-a^{-1}}{z}$ associated to the HOMFLY-PT polynomial.

After this, following the procedure described in Section 3.2, we obtain the specializations of coefficients presented below. We remark that following the setting used from the previous construction, we have as image for the specialization map the ring of Laurent polynomials in Q . In this situation, it means that in the above two cases associated to α_J^σ and α_H^σ we would have polynomials in the variables $1 - q - q^{-1}$ (and $1 - \frac{a-a^{-1}}{z}$ respectively) and their inverses.

However, we will enlarge slightly the ring of coefficients and look at the following specializations.

Definition 3.22 (Specialization of coefficients for the Jones polynomial). We have the change of coefficients:

$$(27) \quad \alpha_J^\sigma: \mathbb{Z}[x_1^{\pm 1}, \dots, x_{8n}^{\pm 1}] \rightarrow \mathbb{Z}[q^{\pm 1}](1 - q - q^{-1})$$

and the associated specialized intersection pairing:

$$(28) \quad \langle\langle \cdot, \cdot \rangle\rangle_{\alpha_J^\sigma}: \mathcal{H}_{2n}^{lf} |_{\alpha_J^\sigma} \otimes \mathcal{H}_{2n} |_{\alpha_J^\sigma} \rightarrow \mathbb{Z}[q^{\pm 1}](1 - q - q^{-1}).$$

Definition 3.23 (Specialization of coefficients for the HOMFLY-PT polynomial). For the case of the HOMFLY-PT polynomial we will use the change of coefficients:

$$(29) \quad \alpha_H^\sigma : \mathbb{Z}[x_1^{\pm 1}, \dots, x_{8n}^{\pm 1}] \rightarrow \mathbb{Z}[a^{\pm 1}, z^{\pm 1}] \left(1 - \frac{a - a^{-1}}{z}\right)$$

and the associated specialized intersection pairing:

$$(30) \quad \ll , \gg_{\alpha_H^\sigma} : \mathcal{H}_{2n}^{lf} |_H \otimes \mathcal{H}_{2n} |_H \rightarrow \mathbb{Z}[a^{\pm 1}, z^{\pm 1}] \left(1 - \frac{a - a^{-1}}{z}\right).$$

4. RECOVERING THE JONES POLYNOMIAL

We describe how the intersection pairing with given specialization in the previous section recovers the Jones polynomial.

4.1. The Kauffman bracket and the Jones polynomial. Let L be a link in S^3 with diagram D . For a plane S^2 of projection for a diagram of L , the Kauffman bracket skein module [18] $K(S^2)$ is the complex vector space generated by unoriented link diagrams, considered up to planar isotopy and modulo the Kauffman bracket skein relations:

- the simple unknot $\bigcirc = (q + q^{-1})$;
- let D be an unoriented link diagram and let χ represent a crossing \times in D , then

$$D = D_\chi = \sqrt{-q^{-1}}D_+ + \sqrt{-q}D_-.$$

Here D_+ and D_- are link diagrams that are identical to $D = D_\chi$ everywhere outside of a small neighborhood of the crossing χ , and they differ from D in the small neighborhood as indicated in Figure 8.



FIGURE 8. The resolutions at each crossing.

Remark 4.1. We remark that we are not using the standard normalization for the skein relation.

The *Kauffman bracket* $\langle D \rangle$ is the Laurent polynomial in q multiplying the empty diagram after removing every crossing of D and closed circle components using the Kauffman bracket skein relations. The writhe $w(D)$ of a link diagram D is the sum of the signs of the positive and negative crossings of D . We give a definition of the (unreduced) Jones polynomial [14] using the Kauffman bracket.

Definition 4.2. Let D be the diagram of an oriented link L with orientation forgotten. The Jones polynomial $J_L(q)$ of the link L is given by

$$(31) \quad J_L(q) = (-q)^{\frac{3w(D)}{2}} \langle D \rangle.$$

Given a Kauffman state σ , let $n_+(\sigma)$ be the number of $+$ -resolutions chosen by σ and $n_-(\sigma)$ be the number of $-$ -resolutions chosen by σ . Define $\text{sgn}(\sigma) := n_+(\sigma) - n_-(\sigma)$. Recall that a Kauffman state chooses the $+$ - or the $-$ -resolution at each crossing of a link diagram D (Definition 3.9). Applying a Kauffman state σ to a link diagram, replacing every crossing by the chosen resolution results in a disjoint collection of circles S_σ . Let $|\sigma|$ be the number of circles in the collection. The Kauffman bracket $\langle D \rangle$ can be defined in terms of a *state sum*:

$$(32) \quad \langle D \rangle = \sum_{\sigma \text{ a Kauffman state on } D} q^{\frac{-\text{sgn}(\sigma)}{2}} (q + q^{-1})^{|\sigma|}.$$

Therefore,

$$(33) \quad J_L(q) = (-1)^{\frac{3w(D)}{2}} \sum_{\sigma \text{ a Kauffman state on } D} q^{\frac{-\text{sgn}(\sigma) + 3w(D)}{2}} (q + q^{-1})^{|\sigma|}.$$

We remark that the writhe already has a geometric meaning as the self-intersection of the link diagram.

Definition 4.3 (Collections of arcs and ovals). Let us suppose that we have a fixed Kauffman state σ . For the following model, we keep the set of blue arcs, but we replace the black arcs by green ovals, which are constructed in a tubular neighbourhood of these arcs, as in Figure 9. With this data, we denote:

- $F(\sigma)$ to be the set of blue arcs associated to the state, and
- $L(\sigma)$ to be the set of green ovals constructed from the black arcs associated to our state.

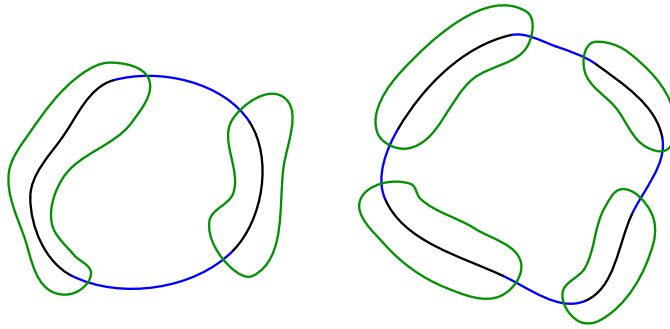


FIGURE 9. The collection of green ovals replacing the black arcs.

Definition 4.4 (Orientation). We fix an orientation for our arcs and ovals. First, we orient all the ovals such that their orientations are consistent with the counter-clockwise orientation. For the arcs, we orient them such that each pair that comes from a resolution has the orientation as in Figure 10.

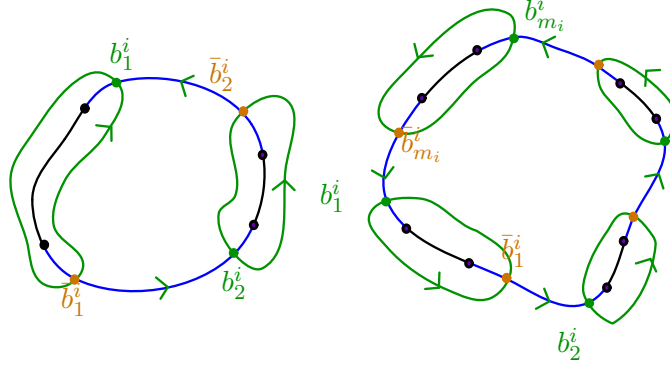


FIGURE 10. Homology classes for the Jones polynomial: $\mathcal{F}(\sigma), \mathcal{L}(\sigma)$.

Now we fix an orientation for our surface such that the base points from Figure 10 have all positive orientation.

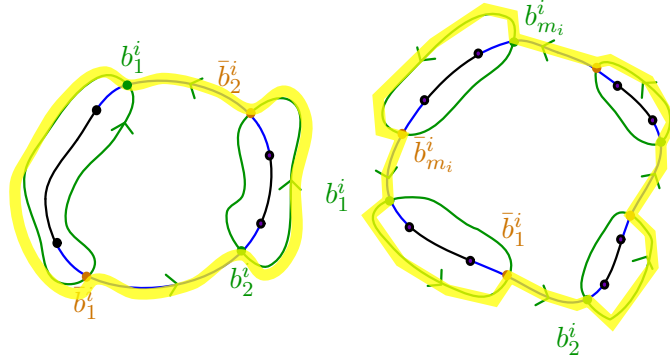


FIGURE 11. A loop l_x in the configuration space, highlighted in yellow.

4.2. Homology classes associated to a state. The next part of our construction is devoted to the definition of two homology classes coming from the two collections of arcs and ovals associated to a fixed Kauffman state.

General method for obtaining homology classes.

One can obtain homology classes from the following data:

- A *geometric support*, given by a *collection of arcs or ovals in the punctured disk*. Then, the image of the product of these arcs or ovals in the configuration space $C_{2n}(\Sigma')$ leads to a submanifold (which has half of the dimension of the configuration space, so dimension n).
- A collection of *paths to the base point*, which start in the base points from the punctured surface $\{b_1, \dots, b_{2n}\}$ and end on these curves. The set of all these paths leads to a path in the configuration space, from the base point \mathbf{d} to the submanifold.

Then, the procedure is to lift the path to a path in the covering of the configuration space, that starts from $\tilde{\mathbf{d}}$ (which is our fixed left of the base point \mathbf{d}). After that, we lift the submanifold through the end point of this path. The detailed construction of such homology classes is presented in [2].

In our situation, we will construct the ovals such that they pass through the base points, as presented in Figure 10. We recall that locally, at each crossing, our base points are chosen near the punctures x_l and y_r . Since the ovals are obtained from the α arcs also by a deformation, we can choose them such that they pass through the base points. For the α arcs, we notice that they also contain the base point.

Definition 4.5 (Homology classes for the Jones polynomial). With this procedure the collection of curves $F(\sigma)$ leads to a homology class in the covering, which we denote as

$$\mathcal{F}(\sigma) \in \mathcal{H}_{2n}^{lf}.$$

Dually the collection of ovals $L(\sigma)$ leads to a homology class in the covering, which we denote as

$$\mathcal{L}(\sigma) \in \mathcal{H}_{2n} \text{ (Figure 10).}$$

4.3. Intersection of classes recovers the evaluation of state circles.

In this part we put all the ingredients together and show that through the topological tools that we introduced above we can obtain the evaluation of the Kauffman bracket on a set of state circles.

Intersection for generic parameter Q . We first show that for a given Kauffman state σ , the intersection between the associated homology classes recovers a polynomial raised to the power given by the number of circles $|\sigma|$, as below.

Lemma 4.6 (Recovering the Kauffmann bracket in a general form). *We work in the context where we have an indeterminate Q and the associated specialization α_Q^σ . Fix a state σ . Then, the intersection between the classes $\mathcal{F}(\sigma)$ and $\mathcal{L}(\sigma)$ specialized through α_Q^σ gives a fixed polynomial in Q to the number of circles, as below:*

$$(34) \quad \ll \mathcal{F}(\sigma), \mathcal{L}(\sigma) \gg_{\alpha_Q^\sigma} = (1 - Q)^{|\sigma|}.$$

Proof. We will use the formula for computing the intersection.

Step 1- Reducing the problem to the case of a single state circle

Consider the geometric supports of the homology classes $\mathcal{F}(\sigma)$ and $\mathcal{L}(\sigma)$: they are given by lifting the collection of arcs $F(\sigma)$ and the collection of ovals $L(\sigma)$ to the configuration space. We remark that these two collections of arcs and ovals on the surface contain the set of state circles associated to σ . The intersection between $\mathcal{F}(\sigma)$ and $\mathcal{L}(\sigma)$ is parameterized by the set

of intersection points between their geometric supports, and then graded by the local system.

Consider the set of intersection points. Such a point is encoded by a $(2n)$ -tuple of points $z = (z_1, \dots, z_{2n})$ on the surface Σ' such that:

- (1) each arc from $F(\sigma)$ contains exactly one component from the set $\{z_1, \dots, z_{2n}\}$
- (2) each oval from $L(\sigma)$ contains exactly one component from the set $\{z_1, \dots, z_{2n}\}$.

Note the above requirement gives conditions on the intersection points between the collections of arcs and ovals that contain the same state circle. So, in order to have an intersection point $z = (z_1, \dots, z_{2n})$ we should choose for each state C_i (which is bicolored into let's say $2m_i$ components) m_i points on the punctured surface $(z_1^i, \dots, z_{m_i}^i)$ with the following requirement:

- (1) each arc from $F(\sigma)$ bounding C_i contains exactly one component from the set $\{z_1^i, \dots, z_{m_i}^i\}$;
- (2) each oval from $L(\sigma)$ bounding C_i contains exactly one component from the set $\{z_1^i, \dots, z_{m_i}^i\}$.

Then our intersection point z will be given by the collection of chosen points $z^i = (z_1^i, \dots, z_{2m_i}^i)$ associated to each state circle:

$$\{z_1^i, \dots, z_{2m_i}^i \mid 1 \leq i \leq |\sigma| \}.$$

Now, for our intersection we have to compute two parts:

- i) the loop l_z and its evaluation through the local system
- ii) the sign α_z .

The sign will be the product of signs associated to each component from the set of state circles.

The main remark that is used for the next step is that given the property that the intersection point has its components separated into components associated to the state circles, the loop l_z and then its evaluation through the local system are both obtained from separate components associated to each state circle separately. For $\Phi(l_z)$ we compute the contribution of each loop associated to a state circle l_{z^i} and consider the product of all of these when we evaluate the monodromies around the punctures through the local system and then the specialization.

Step 2- Intersection points associated to one state circle

As explained in Step 1, the intersection between our two homology classes can be computed by investigating each individual state circle and computing its contribution to the monodromy of the local system, as below.

Lemma 4.7 (Intersection points along a closed component). *Let us fix a state circle C_i . Then, there are exactly two choices for the intersection points associated to this component: $\bar{B}^i = (\bar{b}_1^i, \dots, \bar{b}_{m_i}^i)$ or $\bar{B}^i = (\bar{\bar{b}}_1^i, \dots, \bar{\bar{b}}_{m_i}^i)$.*

Proof. First, we look at the components of the base point \mathbf{d} that belong to this state circle and denote them as: $(\bar{b}_1^i, \dots, \bar{b}_{m_i}^i)$.

Let us denote by:

- $F^i(\sigma)$ the set of arcs from $F(\sigma)$ bounding C_i
- $L^i(\sigma)$ the set of ovals from $L(\sigma)$ bounding C_i .

Requirement for intersection points

We have seen that an intersection point associated to a component C_i is given by a choice of $2m_i$ points on the punctured surface $(z_1^i, \dots, z_{m_i}^i)$ with the following requirement:

- (1) each arc from $F^i(\sigma)$ contains exactly one component from the set $\{z_1^i, \dots, z_{m_i}^i\}$
- (2) each oval from $L^i(\sigma)$ contains exactly one component from the set $\{z_1^i, \dots, z_{m_i}^i\}$.

We remark that we have a set of special points that belong to our collection of arcs and ovals:

$$(\bar{b}_1^i, \dots, \bar{b}_{m_i}^i).$$

Following our construction, we remark that these base points, when following the state circle, are chosen at interval at Step 2, as illustrated in Figure 10. This means that

$$\bar{B}^i = (\bar{b}_1^i, \dots, \bar{b}_{m_i}^i)$$

provides a well defined intersection point that satisfies the above **Requirement for intersection points**.

Now, we investigate which other intersection points satisfy this requirement. Consider the oval containing \bar{b}_1^i . If for this oval we do not choose the intersection point \bar{b}_1^i , we are obliged to choose the other point at the intersection with the next arc. Let us denote this point by $\bar{\bar{b}}_1^i$. Then, we look at the following oval, containing the base point \bar{b}_2^i . We have to choose a component belonging to this oval as well. It cannot coincide with \bar{b}_2^i , since \bar{b}_2^i and \bar{b}_1^i belong to the same arc. So we have to choose the next point, which we denote by $\bar{\bar{b}}_2^i$. Following this inductive procedure, we see that all components are prescribed by the choice of the point $\bar{\bar{b}}_1^i$, and so we have a unique choice for a second intersection point

$$\bar{\bar{B}}^i = (\bar{\bar{b}}_1^i, \dots, \bar{\bar{b}}_{m_i}^i)$$

that satisfies the above requirement. Overall, we see that we have exactly two intersection points: one given by the components close to the base points $\bar{B}^i = (\bar{b}_1^i, \dots, \bar{b}_{m_i}^i)$, and a second one whose components are given by the other possible situation $\bar{\bar{B}}^i = (\bar{\bar{b}}_1^i, \dots, \bar{\bar{b}}_{m_i}^i)$. \square

Step 4- Computing the contribution of the loop associated to one state circle

For this step we aim to compute the contribution of the intersection points \bar{B}^i or $\bar{\bar{B}}^i$ once we evaluate the local system and specialize it through α_Q . For this, we have to see which loops are associated to these intersection points.

a) Intersection point close to the base point

If we have chosen the components of \bar{B}^i , then the loop associated to it is a constant loop whose components are the base points

$$b_1^i, \dots, b_{m_i}^i.$$

We remark that this loop does not wind around any puncture, so the contribution of the intersection point \bar{B}^i to the local system gets evaluated to 1.

b) Intersection point opposite to the base point

If we have chosen the components of $\bar{\bar{B}}^i$, then the loop associated to it starts in the base points

$$(\bar{b}_1^i, \dots, \bar{b}_{m_i-1}^i, \bar{b}_{m_i}^i),$$

continues on the arcs to the components

$$\bar{b}_1^i, \dots, \bar{b}_{m_i}^i$$

and goes back to the “next” base points following the ovals, arriving in

$$(\bar{b}_2^i, \dots, \bar{b}_{m_i}^i, \bar{b}_1^i).$$

We remark that this is a loop in the configuration space whose image on the surface is, up to a little isotopy precisely the state circle C_i . So, its contribution to the local system gets evaluated to the product of monodromies of punctures associated to the state disc D^{C_i} . Following the definition of the change of coefficients α_Q^σ , this product is precisely Q , since α_Q^σ was defined exactly such that it satisfies the **Monodromy Requirement** in Section 3.2.

We conclude that the contribution to the local system of the intersection point $\bar{\bar{B}}^i$ gets evaluated to Q .

Step 4- Sign contribution of intersection points associated to a state circle

For each intersection point z in the configuration space, we have to compute the sign of the intersection between the submanifolds given by $F(\sigma)$ and $L(\sigma)$ at z . This sign is given by:

- (1) the product of the sign of local orientations at the components of z on the surface;
- (2) the sign of the permutation induced by this intersection point on the components of the geometric supports: $F(\sigma)$ and $L(\sigma)$.

a) Sign contribution of the intersection point \bar{B}^i

For the point \bar{B}^i we remark that all intersections between arcs and ovals have positive local orientations and also there is no permutation induced at

the level of the set of arcs and ovals. So this point has a sign contribution of

$$+1.$$

b) Sign contribution of the intersection point $\bar{\bar{B}}^i$

Looking at the second intersection point $\bar{\bar{B}}^i$, we remark that all intersections between arcs and ovals have negative local orientations. This gives the sign:

$$(-1)^{m_i}.$$

Also the permutation induced by its components can be seen by checking the permutation induced by the associated loop on the base points. This, as we have seen, is a cyclic permutation of order m_i , which has the signature $(-1)^{m_i-1}$. So, the sign coming from the permutation associated to $\bar{\bar{B}}^i$ is:

$$(-1)^{m_i-1}.$$

Overall, the point $\bar{\bar{B}}^i$ carries the sign:

$$(-1)^{m_i-1} \cdot (-1)^{m_i} = -1.$$

Step 5- Contribution of intersection points associated to one circle to the intersection form

Overall for our two points we obtain the following contributions:

- (1) $\bar{\bar{B}}^i$: contributes to the local system evaluation by 1 and carries the sign 1.
- (2) $\bar{\bar{B}}^i$: contributes to the local system evaluation by $-Q$ and carries the sign -1 .

This shows that the component C_i gives two possible choices for components of intersection points, and each of them gets weighted by the monomials presented above. This means that this component contributes to the intersection by the sum of these two weights, which is precisely:

$$(35) \quad 1 + (-1) \cdot Q = 1 - Q.$$

Doing this procedure for all state circles, and we have $|\sigma|$ of them, we obtain that our intersection is indeed:

$$(36) \quad \ll F(\sigma), L(\sigma) \gg_{\alpha_Q^\sigma} = (1 - Q)^{|\sigma|}.$$

which concludes the proof of the Lemma. □

Now we are ready to put together all the previous set-up and show that we have defined the right topological model, provided by the set of graded intersections of homology classes which, for the appropriate choice of specialization of coefficients lead to the Jones polynomial and to the HOMFLY-PT polynomial, respectively.

4.4. Intersection form recovering the evaluation on closed components. Recall that in Definition 3.22 we have introduced the change of coefficients

$$(37) \quad \alpha_J^\sigma : \mathbb{Z}[x_1^{\pm 1}, \dots, x_{8n}^{\pm 1}] \rightarrow \mathbb{Z}[q^{\pm 1}](1 - q - q^{-1}).$$

This gives the associated specialized intersection pairing:

$$(38) \quad \ll , \gg_{\alpha_J^\sigma} : \mathcal{H}_{2n}^{lf} |_{\alpha_J^\sigma} \otimes \mathcal{H}_{2n} |_{\alpha_J^\sigma} \rightarrow \mathbb{Z}[q^{\pm 1}](1 - q - q^{-1}).$$

Lemma 4.8 (Recovering the Kauffman bracket via intersections of arcs and ovals). *Fix a state σ . Then, the intersection between the classes $\mathcal{F}(\sigma)$ and $\mathcal{L}(\sigma)$ specialized through α_J^σ gives precisely the Kauffman bracket evaluated on the state σ :*

$$(39) \quad \ll \mathcal{F}(\sigma), \mathcal{L}(\sigma) \gg_{\alpha_J^\sigma} = (q + q^{-1})^{|\sigma|}.$$

Proof. Following Lemma 4.6, we have that:

$$(40) \quad \ll \mathcal{F}(\sigma), \mathcal{L}(\sigma) \gg_{\alpha_Q^\sigma} = (1 - Q)^{|\sigma|}.$$

In our case we have $Q = Q_J = 1 - q - q^{-1}$ and so this leads to our desired formula for the intersection:

$$(41) \quad \ll \mathcal{F}(\sigma), \mathcal{L}(\sigma) \gg_{\alpha_J^\sigma} = (q + q^{-1})^{|\sigma|}.$$

□

4.5. A topological model for the Jones polynomial. In this section, we obtain a topological model of the Jones polynomial by defining Θ_J and proving Theorem 2. To define Θ_J , recall the Jones polynomial of an oriented link may be defined in terms of the Kauffman bracket (Definition 4.2) of a diagram D of the link with orientation forgotten:

$$(42) \quad J_L(q) = (-1)^{\frac{-3w(D)}{2}} \sum_{\sigma \text{ a Kauffman state on } D} q^{\frac{-\text{sgn}(\sigma) + 3w(D)}{2}} (q + q^{-1})^{|\sigma|}.$$

Since Lemma 4.6 recovers $(q + q^{-1})^{|\sigma|}$ as the intersection pairing $\ll , \gg_{\alpha_{Q_J}^\sigma}$ for each Kauffman state σ , it remains to give a geometric interpretation of the monomial $q^{\frac{-\text{sgn}(\sigma) + 3w(D)}{2}}$.

Let \mathcal{A} denote the set of α -curves and let \mathcal{B} denote the β -curves. At each crossing x , we distinguish a pair of the α -curves by whether they give the oriented resolution or the non-oriented resolution. They are denoted by $\alpha_o(x)$ for the oriented resolution, $\alpha_\delta(x)$ for the non-oriented resolution, respectively. Let σ be a Kauffman state on a digram D of L , we twist the alpha curves by σ as follows.

If x is positive: If σ chooses the 0-resolution at the crossing, then replace by the twisted α_o -arcs as indicated in Figure 12. If σ chooses the 1-resolution, then replace by the α_δ -arcs (without twisting).

If x is negative: If σ chooses the 1-resolution at the crossing, then replace by the twisted α_σ -arcs as indicated in Figure 12. If σ chooses the 0-resolution, then replace by the α_σ -arcs (without twisting).

We denote the set of curves resulting from this twisting by $D_\sigma(\alpha)$.

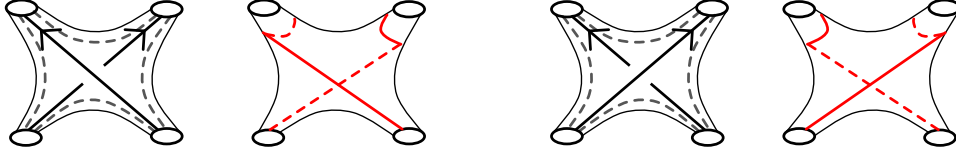


FIGURE 12. Depending on the sign of the crossing, we twist the pair of alpha curves corresponding to the oriented resolution at a crossing to the red curves shown. A dashed red line is on the back of the surface, and a solid red line is on the front of the surface.

Lemma 4.9. *The degree $\frac{-\text{sgn}(\sigma)+3w(D)}{2}$ of the monomial of q in (42) is given by the oriented geometric intersection $i(D_\sigma(\alpha), D)$ of $D_\sigma(\alpha)$ with the link diagram D :*

$$\frac{-\text{sgn}(\sigma) + 3w(D)}{2} = -\frac{i(D_\sigma(\alpha), D)}{2} + w(D).$$

Remark 4.10. Note $D_\sigma(\alpha)$ may be written in terms of the homology classes of loops around the punctures on the 4-punctured spheres, but it may not necessarily lift to the configuration space if it does not evaluate to 0, which is why it is not part of the intersection form $\ll, \gg_{\alpha_\sigma^j}$ defined in Section 4.4.

Proof. We adapt the proof in [10] to our setting. Recall $\text{sgn}(\sigma) = n_+(\sigma) - n_-(\sigma)$, where $n_+(\sigma)$ is the number of crossings of D on which σ chooses the $+$ -resolution, and $n_-(\sigma)$ is the number of crossings of D on which σ chooses the $-$ -resolution. Finally, $n(D)$ is the number of crossings in the set of crossings $c(D)$ of D .

The writhe $w(D) = n^+(D) - n^-(D)$ is the difference of the number of positive crossings of D with the number of negative crossings of D .

Let $n_-^+(\sigma)$ be the number of crossings on which σ chooses the $-$ -resolution at a positive crossing, and let $n_+^-(\sigma)$ be the number of crossings on which σ chooses the $+$ -resolution at a negative crossing.

Then,

$$\text{sgn}(\sigma) - w(D) = n_+(\sigma) - n_-(\sigma) - (n^+(D) - n^-(D)).$$

Decomposing

$$n_+(\sigma) = n_-^+(\sigma) + n_+^+(\sigma), \quad n_-(\sigma) = n_-^-(\sigma) + n_+^-(\sigma)$$

and

$$n^+(D) = n_+^+(\sigma) + n_-^+(\sigma), \quad n^-(D) = n_+^-(\sigma) + n_-^-(\sigma),$$

we obtain

$$\begin{aligned} \operatorname{sgn}(\sigma) - w(D) &= n_+(\sigma) - n_-(\sigma) - (n^+(D) - n^-(D)) \\ &= n_+^-(\sigma) + n_+^+(\sigma) - (n_-^-(\sigma) + n_-^+(\sigma)) - (n_+^+(\sigma) + n_-^+(\sigma) - (n_+^-(\sigma) + n_-^-(\sigma))) \\ &= 2n_+^-(\sigma) - 2n_-^+(\sigma). \end{aligned}$$

Thus we can rewrite

$$\frac{\operatorname{sgn}(\sigma) - 3w(D)}{2} = \frac{\operatorname{sgn}(\sigma) - w(D) - 2w(D)}{2} = \frac{2n_+^-(\sigma) - 2n_-^+(\sigma)}{2} - w(D).$$

Now consider the σ -state surface Σ_σ of the link L with diagram D . The boundary of the surface Σ_σ is isotopic to $D_\sigma(\alpha)$ by construction, and $i(D_\sigma(\alpha), D)$ counts the geometric intersection, or, linking number, between $D_\sigma(\alpha)$ and D by definition. We claim

$$i(D_\sigma(\alpha), D) = 2n_+^-(\sigma) - 2n_-^+(\sigma) = \operatorname{sgn}(\sigma) - w(D),$$

since we can compute the linking number by summing over the local contributions. On a positive crossing where σ chooses the $+$ -resolution, there is 0 intersection between $D_\sigma(\alpha)$ and D . Similarly for a negative crossing on which σ chooses the $-$ -resolution, there is no intersection between $D_\sigma(\alpha)$ and D . In the rest of the cases the intersection contributes ± 2 to the linking number, as illustrated in Figure 13. \square

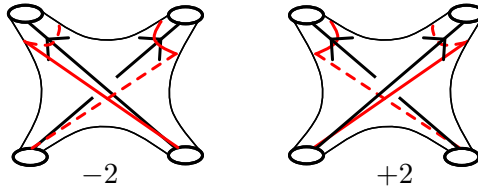


FIGURE 13. Left: choosing the $+$ -resolution contributes -2 to the oriented intersection at a negative crossing; Right: choosing the $-$ -resolution contributes to $+2$ to the oriented intersection at a positive crossing.

We are now ready to prove Theorem 2.

4.6. Proof of Theorem 2. Let $i(D_\sigma(\alpha), D)$ be the geometric intersection between the curve $D_\sigma(\alpha)$ and the link diagram D defined in the previous section, Section 4.5, $w(D)$ be the writhe of D , and \ll, \gg_{α^σ} be the intersection pairing defined in Section 4.4.

Definition 4.11 (Intersection form for the Jones polynomial). Let $F(\sigma)$, $L(\sigma)$ be two collections of curves defined (Definition 4.3) and evaluated by the specialized intersection pairing as in Section 4.4. The function $\Theta_J(D)$ is defined as

$$\Theta_J(D) := \sum_{\sigma \text{ a Kauffman state}} q^{\frac{-i(D_\sigma(\alpha), D) + 3w(D)}{2}} \ll \mathcal{F}(\sigma), \mathcal{L}(\sigma) \gg_{\alpha_J^\sigma}.$$

We restate Theorem 2 for the convenience of the reader.

Theorem 4.12 (Theorem 2) (Topological model for the Jones polynomial from link diagrams).

Let $\Theta_J(D) \in \mathbb{Z}[q^\pm]$ be state sum of graded intersections in the same configuration space on our fixed Heegaard surface, as defined in Definition 1.4. Then it provides a topological model for the Jones polynomial, relying just on the choice of a diagram D :

$$\Theta_J(D) = J_L(q).$$

Proof. By Lemma 4.9, $q^{\frac{-i(D_\sigma(\alpha), D) + w(D)}{2}}$ in Θ_J recovers $q^{-\frac{\text{sgn}(\sigma) + 3w(D)}{2}}$ in the Kauffman state sum definition (42) of the Jones polynomial. Lemma 4.8 implies that the term $\ll F(\sigma), L(\sigma) \gg_{\alpha_J^\sigma}$ recovers $(q + q^{-1})^{|\sigma|}$ in the state sum definition. It follows that Θ_J recovers the Jones polynomial. \square

5. RECOVERING THE HOMFLY-PT POLYNOMIAL

The HOMFLY-PT polynomial satisfies the following skein relations and recovers the Jones polynomial and the Alexander polynomial through specializations of its variables.

$$(43) \quad aP(\text{crossing}) - a^{-1}P(\text{crossing}) = zP(\text{split}) \quad P(U) = 1$$

Here U denotes the standard projection of the unknot on the projection plane. Suppose U^m is an unlink with m components, then

$$P(U^m) = \left(\frac{a - a^{-1}}{z} \right)^{m-1}.$$

We recover the Jones polynomial $J_L(q)$ and the symmetrized Alexander polynomial $\Delta_L(t)$ through the following specializations:

$$\begin{aligned} J_L(t) &= P(L)|_{a=q^{-2}, z=q^{-1}} \\ \Delta_L(t) &= P(L)|_{a=1, z=t^{1/2}-t^{-1/2}}. \end{aligned}$$

In this section we describe a topological model for the HOMFLY-PT polynomial from intersections of curves on a Heegaard surface. The common ingredient for the construction is a state sum model, which is given by the Kauffman bracket for the Jones polynomial, and in the case of the HOMFLY-PT polynomial is given by the skein relation (43).

5.1. Descending diagrams. We recall an algorithm for applying the skein relation (43) to compute the HOMFLY-PT polynomial using a sum over descending link diagrams. For the original reference, see [11] for Hoste's construction of the HOMFLY-PT polynomial and the argument that it is a link invariant using descending diagrams. The definition of nondescending complexity $nd(D)$ used in this paper is due to Murasugi and Przytycki [16].

We define a subset $nd(D)$ of the crossings to represent the non-descending complexity of the diagram D .

Definition 5.1. Let $D = D_1, \dots, D_k$ be an ordering of the components of an oriented link diagram D , and let $\{\ell_1, \dots, \ell_k\}$ where $\ell_i \in D_i$ be a set of base points (note: different from the base points b_i considered previously) that avoid double points of crossings in D . Define $r(D)$ to be the set of crossings reached by traversing each component of the link in given order starting with ℓ_1 on D_1 , where we terminate the travel before a nonnugatory crossing is met for the first time, and the strand being traversed is under another link strand at the crossing. A crossing of D is in $nd(D)$ if it is not in $r(D)$.

The number of crossings in $nd(D)$, denoted by $|nd(D)|$, represents the nondescending complexity of D . If $nd(D)$ is empty, so there is no nondescending complexity, then D is called a *descending diagram*. A descending link diagram represents an unlink where the component D_j is below D_i if $j > i$.

With a suitable choice of base points and ordering of link components, the HOMFLY-PT polynomial of a link with diagram D can be evaluated as a sum of unlinks through applying the skein relation (43) to D , in a way that $|nd(D')|$ of intermediate diagrams D' decreases at every step until it reaches 0. The sum of unlinks with polynomial coefficients in two variables from a skein relation of the HOMFLY-PT polynomial gives a state sum model, see Jaeger [12].

We describe how to apply the skein relation (43) to reduce the polynomial to a sum of the HOMFLY-PT polynomial of unlinks. Following the description of [8], the first step is to choose an ordering of components and a set of base points for the diagrams involved in applying the relation.

Choice of ordering of components and base points for decreasing $|nd(D)|$. Let D be an oriented link diagram with components D_1, \dots, D_ℓ and base points b_1, \dots, b_ℓ such that $b_i \in D_i$. Given a (positive or negative) crossing χ in D , let $-\chi$ be the crossing with opposite sign (negative or positive). Applying (43) expands the HOMFLY-PT polynomial of the link represented by $D = D_\chi$ in terms of the HOMFLY-PT polynomial of two link diagrams $D_{-\chi}$ and D_o , where $D_{-\chi}$ is obtained by locally replacing χ by $-\chi$, and D_o is obtained by replacing χ by two arcs from the oriented resolution of χ .

Assume $nd(D)$ is not empty, and let i be the smallest index for which D_i has a crossing that is in $nd(D)$. Let $\chi \in nd(D)$ be the crossing in D_i just after the traversal on D_i terminates, so χ is the first crossing included in $nd(D)$.

We choose the following ordering of components and base points of $D_{-\chi}$ and D_o so that the descending complexity $|nd|$ strictly decreases through each application of the skein relation. That is, $|nd(D_{-\chi})| < |nd(D)|$ and $|nd(D_o)| < |nd(D)|$.

- (1) The diagram $D_{-\chi}$ inherits base points and ordering of components from D_χ : a component of $D_{-\chi}$ has the same base point and ordering as the corresponding component in D_χ that is identical to the component outside of χ .
- (2) There are two cases for D_o . Either
 - (a) **replacing by the oriented resolution at χ splits a component D_i of D into two components D_A, D_B in D_o**
 For $j < i$, let each component in D_o corresponding to D_j inherit the same base point and order as D_j . Let the new component D_A inherit the same base point as D_i in D and choose a base point on the new component D_B just before the crossing χ . Number component D_A by i , component D_B by $i + 1$, and renumber each component in D_o corresponding to D_j for $j > i$ by shifting each index by 1, sending $j \mapsto j + 1$.
 - (b) **replacing by the oriented resolution at χ merges two component $D_i, D_k, i < k$, of D into one component D_A in D_o .**
 Let the new component D_A inherit the same base point as D_i and number it i . For $j \neq i$ such that $j < k$, let each component in D_o corresponding to D_j inherit the same base point and order as D_j . Renumber the components corresponding to D_j for $j > k$ by sending $j \mapsto j - 1$.

Lemma 5.2. *Let D be a link diagram with a set of base points $\{b_1, \dots, b_\ell\}$ and an ordering of components. Let χ be the first crossing in $nd(D)$. With the choice of base points and ordering as described above for D, D_o , and $D_{-\chi}$, we have*

$$|nd(D_{-\chi})| < |nd(D)| \text{ and } |nd(D_o)| < |nd(D)|.$$

Proof. To show $|nd(D_{-\chi})| < |nd(D)|$, we see that $nd(D_{-\chi})$ has at least one fewer crossing compared to $nd(D)$ since we can now extend travel past the crossing $-\chi$ in $nd(D_{-\chi})$. For $|nd(D_o)| < |nd(D)|$ we again address two cases depending on whether D_o merges a pair of components in D or splits a component in D into two.

Case 1 A single component D_i in D is split into two components numbered $i, i + 1$ in D_o .

To compute $nd(D_o)$ we traverse D_o in order of the newly chosen base points and compare crossings in the traveled portion $r(D_o)$ with that of D . For all

components D_j where $1 \leq j < i$, D and D_o share the same crossings in the traveled portion of the link diagram. For the component numbered i , the traveled portion is now extended past the crossing χ , where it may pick up more crossings in D_o , so $nd(D_o) \leq nd(D) - 1$ and $nd(D_o) < nd(D)$.

Case 2 Two components D_i, D_k in D are merged into a single component in D_o .

Without loss of generality we assume $i < k$. For all components in D_o numbered $j < i$, the traveled portion remains the same. When traversing the i th component of D_o , the crossing χ is removed as we continue to travel on the portion coming from D_k , where additional crossings may be included in $r(D_o)$. Thus we have again $nd(D_o) \leq nd(D) - 1$ so $nd(D_o) < nd(D)$. \square

5.2. Decomposing into a state sum of unlinks. Starting with a link diagram D , let $\chi \in nd(D)$ be the first nonnugatory crossing that is undercrossed by the strand being traversed as described in the previous section. Apply the skein relation at χ to expand $P(D)$ in terms of $P(D_o)$ and $P(D_{-\chi})$.

If $nd(D_o) \neq 0$ or $nd(D_{-\chi}) \neq 0$, repeatedly expand using the skein relation with the first crossing χ_0 in $nd(D_o)$ and χ_- in $nd(D_{-\chi})$. By Lemma 5.2, the nondescending complexity of the diagrams at each level of the expansion strictly decreases. We terminate when all the diagrams in the expansion have 0 nondescending complexity, ie. they are all descending. Finally, we evaluate the HOMFLY-PT polynomial $P(D)$ by summing over the HOMFLY-PT polynomials of the unlinks (represented by the descending diagrams) multiplied by the polynomial coefficients gathered during the application of the skein relations. In [11], Hoste showed that the resulting polynomial is independent of the choice of base points and ordering of components.

The descending collection of unlinks may still have crossings, though the crossings are unimportant in terms of the evaluation of the HOMFLY-PT polynomial. We replace them by the set of state circles from a Kauffman state on the diagram D via the following lemma.

Lemma 5.3 (Renormalized Kauffman state model). *Given a link diagram D^m with m components, there exists a Kauffman state σ_{D^m} on D^m with $|\sigma_{D^m}| = m$ state circles in $S_{\sigma_{D^m}}$.*

Proof. We first consider the case of an 2-component link, and show that we can find a Kauffman state on D^m whose application results in a diagram with two split components.

A diagram of an unlink with two components has an even number of crossings where the strands of the crossing belong to different components. Where the strand of one component crosses over the other component, it must cross back out. Denote of a pair of such crossings by (χ_{in}, χ_{out}) . Separate the first and second components of these pairs into

$$C_{in}(D^m) = \cup \chi_{in} \quad C_{out}(D^m) = \cup \chi_{out}(D^m).$$

Note we choose the pairs such that $C_{in}(D^m) \cap C_{out}(D^m) = \emptyset$. This can be done by keeping track of how one link component crosses in and out of the other link component. Define σ_{D^m} on $C_{in}(D^m) \cup C_{out}(D^m)$ by having it choose the oriented resolution (with respect to the orientation of the crossing in D^m) on $C_{in}(D^m) \cup C_{out}(D^m)$. Replacing each crossing in $C_{in}(D^m) \cup C_{out}(D^m)$ by the choice of the resolution by σ_{D^m} results in two split link components $D_1 \sqcup D_2$ because we have resolved all of the crossings between them, and the application of the Kauffman state to each pair (χ_{in}, χ_{out}) merges than splits a pair of circles while preserving the orientation of the crossing from D^m .

This argument extends to the case of a diagram of a link with $m \geq 2$ components by inducting on m , since we can remove linking between any pair of components by applying σ_H as defined above, repeatedly as necessary, to obtain a split diagram $D_1 \sqcup D^{m-1}$, where D_1 is an unlinked component and D^{m-1} is a link with $m-1$ components, then apply inductive hypothesis to D^{m-1} .

Given a link diagram $D_s^m = K^1 \sqcup \dots \sqcup K^m$ from D^m of m split components from the above argument, we need to define the Kauffman state σ_{D^m} on the remaining crossings that results in a single state circle. The existence of this Kauffman state is known, for example, in [9], but we can give a self-contained argument here.

Pick a crossing in K^1 and name it c_1 . Define σ_H to choose the non-oriented resolution. This will necessarily preserve the single component of the diagram. Replace c_1 by the oriented resolution to obtain a new knot diagram $K_{s_1}^1$. Orient $K_{s_1}^1$, pick another crossing c_2 , and define σ_H to choose the non-oriented resolution with respect to this new orientation on $K_{s_1}^1$. Repeat this process for $K_{s_i}^1$ obtained by replacing the crossing c_i by the nonoriented resolution in $K_{s_{i-1}}^1$ for $i = 2, \dots, |c(K_1)|$. We eventually exhaust all the crossings in K_1 . Move on to the next component K^2 , then $K^3, K^4 \dots, K^m$, after that, and record the choice of the resolution for σ_{D^m} to choose the same. We have extended σ_{D^m} to all the crossings of D^m . \square

We use Lemma 5.3 to give a state sum definition of the HOMFLY-PT polynomial.

Recall that the algorithm for evaluating $P_L(a, z)$ starts with a diagram D of L and traverses each link component of L in order, and applies the skein relation at the first crossing χ not traversed by an overstrand. The application of the skein relation produces two new link diagrams D_o and $D_{-\chi}$ whose non-descending complexity is strictly less than that of D . Then, the algorithm is repeated for each of D_o and $D_{-\chi}$, until the non-descending complexity is reduced to 0 for each of the pair of diagrams produced through the application of the skein relation.

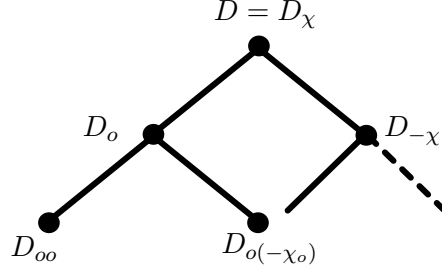


FIGURE 14. The binary tree for applying the HOMFLY-PT skein relation.

It is well known that we can associate a binary tree to the application of this algorithm, see Figure 14 for a depiction. The vertices are D_χ for each such crossing where the skein relation is applied. An edge in the tree starts with D_χ and ends with D_o and $D_{-\chi}$, the two choices of resolution through the skein relation.

Denote by T_D the binary tree associated to a link diagram D , a **state** for the diagram D in this context is the following data associated to a path in T_D that starts at the root (represented by D), and ends at a vertex whose associated link diagram D' has zero nondescending complexity.

Since every link diagram at a vertex of this binary tree T_D inherits crossings from the root diagram D , we will refer to crossings in a link diagram associated to a vertex by their ancestor in D .

Definition 5.4. Let P be a directed path in T_D that starts at the root and ends at a vertex whose associated link diagram has zero non-descending complexity, the **state** σ_H on the diagram D associated to P is a function

$$\sigma_H : c(D) \rightarrow \{o, \hat{o}\}$$

where σ_H makes a choice of the oriented or non-oriented resolution at each crossing of D .

Let e_v be an edge in P whose origin is v and whose terminus is v' . Let $\chi(P)$ be the set of crossings in D on which the algorithm applies the skein relation at a vertex v of the path P in the binary tree T_D . To define σ_H , we first define $\sigma'_H : \chi(D) \rightarrow \{o, -\chi\}$, which is a choice of the oriented resolution or crossing switch at $\chi \in \chi(D)$.

$$\sigma'_H(\chi_v) := \begin{cases} o & \text{if } D_{v'} \text{ is obtained from } D_v \text{ by choosing the oriented resolution at } \chi. \\ -\chi & \text{if } D_{v'} \text{ is obtained from } D_v \text{ by switching the sign of the crossing at } \chi. \end{cases}$$

Replacing a crossing by the choice of the oriented resolution or the crossing switch of $\sigma'_H(\chi_v)$ results in a link diagram with nondescending complexity 0. See Figure 15 for an example of such a state on a diagram of 4_1 .

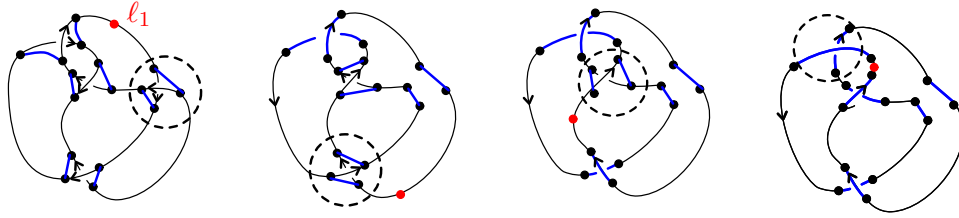


FIGURE 15. The choice of resolutions of σ'_H . The base point ℓ_1 is marked in red as it travels through the diagram. Each crossing encountered that is undercrossed by the strand being traversed is enclosed by a dashed circle.

Let D_f represent the descending link diagram associated to the end vertex of the path P , and let σ_{D_f} be the Kauffman state on D_f that exists by Lemma 5.3. We extend σ_{D_f} and σ'_H to define a Kauffman state σ_H on D as follows:

$$\sigma_H(\chi) := \begin{cases} o & \text{if } \chi \in \chi(D) \text{ and } \sigma'_H(\chi) = o \\ \hat{o} \text{ or } o & \text{if } \chi \notin \chi(D) \text{ and } \sigma_{D_f}(\chi) = \hat{o} \text{ or } o, \text{ respectively} \\ \hat{o} \text{ or } o & \text{if } \chi \in \chi(D) \text{ and } \sigma_{D_f}(\chi) = \hat{o} \text{ or } o, \text{ respectively} \end{cases}$$

We illustrate an example of the state σ_H by further replacing crossings in the descending diagram obtained by applying the state σ_{D_f} to D in Figure 15.

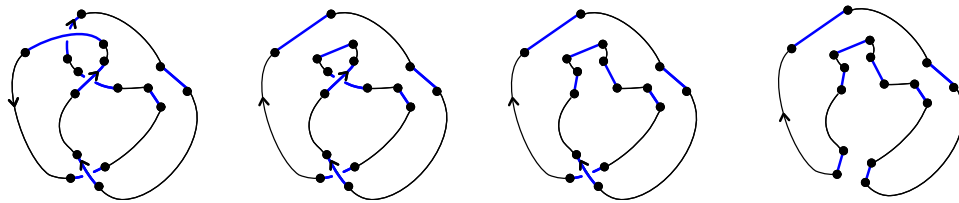


FIGURE 16. Applying σ_H on the remaining crossings in D_f results in a collection of Kauffman state circles with the same number of components as D_f .

Now let $\sigma_H(a, z)$ be the product of coefficients in variables a, z along the path defining σ_H , and let D^{σ_H} represent the diagram of $|\sigma_H|$ component unlinks at the terminal vertex of the path P defining σ_H , then we obtain

$$P_L(a, z) = \sum_{\sigma_H \text{ a state on the diagram } D} \sigma(a, z) P_{D^{\sigma_H}}(a, z).$$

By Lemma 5.3, $P_{D^{\sigma_H}}(a, z) = P_{U^{|\sigma_H|}}(a, z)$, where $U^{|\sigma_H|}$ is the collection of state circles obtained by applying σ_H to D , and $|\sigma_H|$ is the number of circles in the set of circles resulting from applying the state σ_H to every crossing in the diagram D . Therefore

$$(44) \quad \begin{aligned} P_L(a, z) &= \sum_{\sigma_H \text{ a state on the diagram } D} \sigma(a, z) P_{U^{|\sigma_H|}}(a, z) \\ &= \sum_{\sigma_H \text{ a state on the diagram } D} \sigma(a, z) \left(\frac{a - a^{-1}}{z} \right)^{|\sigma_H| - 1}. \end{aligned}$$

5.3. Topological set-up for the HOMFLY-PT polynomial. In this section we construct an intersection model to recover the evaluation of the renormalized Kauffman bracket $P_{U^{|\sigma_H|}}(a, z) = \left(\frac{a - a^{-1}}{z} \right)^{|\sigma_H| - 1}$ on an $|\sigma_H|$ component unlink in the state sum formulation (44) of the HOMFLY-PT polynomial developed in the previous section, as a state sum of Lagrangian intersections on our punctured surface. The idea is to use the above description give by the renormalized Kauffman bracket (as in Lemma 5.3) and translate it homologically as graded intersection between homology classes. For this we need to understand geometrically the meaning of the renormalization taking the number of closed components minus 1, $|\sigma_H| - 1$, rather than $|\sigma_H|$, that appears in the evaluation.

We count intersection points in the configuration space between the following curves:

- the knot diagram
- state circles
- α and β curves

The intersection points are the same as in the model for the Jones polynomial, while we color both the arcs in an unlink from the oriented/non-oriented resolution chosen by σ_H at a crossing blue. See Figure 5. As in Remark 3.10, for each state there are twice as many blue arcs as the number of crossings, and twice as many black arcs as the number of crossings.

Definition 5.5 (Cutting point). Mark one of our base points b_{2n} and call it the “cutting base point” for our diagram.

This is seen by the fact that once we have a set of state circles, the skein relation of the HOMFLY-PT polynomial evaluates all of them but one, instead of evaluating all components. We interpret this topologically by choosing a base point and cutting the diagram in this point. Then, we proceed with the following homology classes.

Definition 5.6 (Collections of arcs and ovals). Suppose that we have a fixed state σ_H . We will follow a similar procedure as the one for the Jones polynomial, the only difference is that we will keep track of our cutting base point.

More precisely, let us keep the set of blue arcs, but we replace the black arcs by ovals, constructed in a tubular neighbourhood of these arcs, as in Figure 17. The important change that we make for this case is that we consider the oval that contains the cutting base point b_{2n} and we deform it to a smaller oval, such that it contains just one puncture, instead of two, as in the picture.

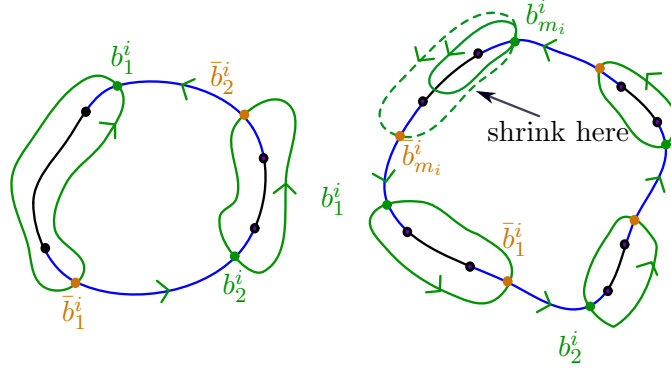


FIGURE 17. Homology classes for HOMFLY-PT polynomial

The effect is that this oval does not intersect the following arc, once we follow the diagram of the link. Now, we consider the following sets:

- $F^H(\sigma_H)$: given by the blue arcs associated to the state
- $L^H(\sigma_H)$ the collection of green ovals constructed from our coloring.

Definition 5.7 (Orientation). We fix an orientation for the arcs and ovals. All the ovals have the counter-clockwise orientation, and for the arcs, we orient them locally as in the case for the Jones polynomial. Each pair that comes from a resolution has the orientation as in Figure 17. We orient our surface such that the base points all have positive orientation.

Homology classes associated to a state. Following the philosophy that we saw for the case of the Jones polynomial, once we have two collections of arcs and ovals associated to a fixed state, we can prescribe two homology classes, using

- 1) the *geometric support*, given by a *collection of arcs or ovals in the punctured disc*.
- 2) the collection of *paths to the base point*, which start in the base points from the punctured surface $\{b_1, \dots, b_{2n}\}$ and end on these curves.

Definition 5.8. With this procedure the collection of curves $F^H(\sigma_H)$ leads to a homology class in the covering, which we denote as

$$\mathcal{F}^H(\sigma_H) \in \mathcal{H}_{2n}^{lf}.$$

Dually the collection of ovals $L^H(\sigma_H)$ leads to a homology class in the covering, which we denote as

$$\mathcal{L}^H(\sigma_H) \in \mathcal{H}_{2n}.$$

5.4. Intersection of classes recovers the evaluation of state circles.

In this section, we show that through the topological setup from above we can obtain the evaluation of circles given by the normalized Kauffman bracket for the HOMFLY-PT polynomial.

The new aspect of this topological viewpoint is that in this case, for a state σ_H , the intersection between the homology classes recovers the polynomial $\left(\frac{a-a^{-1}}{z}\right)$ raised to the power given by the **number of circles minus one**.

Lemma 5.9 (Recovering the normalized Kauffmann bracket in a general form). *Let σ_H be a state. Fix an indeterminate Q and the associated specialization $\alpha_Q^{\sigma_H}$. Then, the intersection of $\mathcal{F}^H(\sigma_H)$ and $\mathcal{L}^H(\sigma_H)$ specialized through $\alpha_Q^{\sigma_H}$ gives a fixed polynomial in Q to the number of circles minus one.*

$$(45) \quad \ll \mathcal{F}^H(\sigma_H), \mathcal{L}^H(\sigma_H) \gg_{\alpha_Q^{\sigma_H}} = (1 - C)^{|\sigma_H|}.$$

Proof. We will use the formula for computing the intersection form.

The proof of this intersection formula follows a similar strategy as the one presented in Lemma 5.9, the new part is to explain why the geometry of the intersections of the homology classes gives us the number of circles minus one, even as we use the same local system and specialization of coefficients.

We explain the main steps below.

Step 1- Reducing the problem to the case of a state circle

Consider the geometric supports of the homology classes $\mathcal{F}^H(\sigma_H)$ and $\mathcal{L}^H(\sigma_H)$: they are given by the collection of arcs $F(\sigma_H)$ and the collection of ovals $L(\sigma_H)$. We remark that these two collections of arcs and ovals on the surface form the boundary of our state circles associated to σ_H . The intersection between $\mathcal{F}(\sigma_H)$ and $\mathcal{L}(\sigma_H)$ is parametrized by: the set of intersection points between their geometric supports, and then graded by the local system.

Let us look at the set of intersection points. Such a point is encoded by a $(2n)$ -tuple of points $z = (z_1, \dots, z_{2n})$ on the surface Σ'_H such that:

- (1) each arc from $F(\sigma_H)$ contains exactly one component from the set $\{z_1, \dots, z_{2n}\}$
- (2) each oval from $L(\sigma_H)$ contains exactly one component from the set $\{z_1, \dots, z_{2n}\}$.

Note that the above requirement adds conditions on the intersection points between arcs and ovals that bound the same state circle. So, in order to have an intersection point $z = (z_1, \dots, z_{2n})$ we should choose for each state C_i (which is bicolored into let's say $2m_i$ components) m_i points on the punctured surface $(z_1^i, \dots, z_{m_i}^i)$ with the following requirement:

- (1) each arc from $F(\sigma_H)$ bounding C_i contains exactly one component from the set $\{z_1^i, \dots, z_{m_i}^i\}$

- (2) each oval from $L(\sigma_H)$ bounding C_i contains exactly one component from the set $\{z_1^i, \dots, z_{m_i}^i\}$.

Then, our intersection point z will be given by the collection of chosen points $z^i = (z_1^i, \dots, z_{2m_i}^i)$ associated to each state circle:

$$\{z_1^i, \dots, z_{2m_i}^i \mid 1 \leq i \leq |\sigma_H| \}.$$

For our intersection we have to compute two parts:

- i) the loop l_z and its evaluation through the local system
- ii) the sign α_z .

The sign will be the product of signs associated to each component from the set of state circles.

For the next steps, we remark that given the property that the intersection point has its components separated into components associated to the state circles, it means that the loop l_z and then its evaluation through the local system are both obtained from separate components associated to each state circle separately. For the result $\Phi(l_z)$ we can see the contribution of each loop associated to a state circle l_{z^i} and consider the product of all of these when we evaluate the monodromies around the punctures through the local system and then the specialization.

Step 2- Intersection points associated to one state circle.

The main idea from the previous step is that our intersection can be obtained using individual computations for each state circle, by looking at its contribution to the monodromy of the local system.

If we have a state circle that does not contain the cutting base point, then the geometric support of the classes $F(\sigma)$ and $F^H(\sigma_H)$ based on it is the same. Similarly, the geometric support of the classes $L(\sigma)$ and $L^H(\sigma_H)$ based on it the same. So the contribution of this state circle gets evaluated to

$$(46) \quad 1 + (-1) \cdot Q = 1 - Q.$$

This follows by an analogous computation as the one presented in Steps 2, 3, and 4 from the proof or Lemma 5.9.

Step 3- Intersection points associated to the circle containing the cutting point

It remains to compute the contribution of the state circle that contains the base cutting point. The subtlety is that in this case the geometric supports for $\mathcal{L}(\sigma)$ and $\mathcal{L}^H(\sigma_H)$ are different (even if the support of $\mathcal{F}(\sigma)$ and $\mathcal{F}^H(\sigma_H)$ is the same).

Lemma 5.10 (Intersection points along the component). *Let us fix the above state circle C_i . Then, there is precisely one intersection point associated to this component: $\bar{B}^i = (\bar{b}_1^i, \dots, \bar{b}_{m_i}^i)$.*

Proof. First, we look at the components of the base point \mathbf{d} that belong to this state circle and denote them as: $(b_1^i, \dots, b_{m_i}^i)$. Let us suppose that our cutting point b_m is $b_{m_i}^i$ from the above notation. We consider:

- $F^i(\sigma_H)$ the set of arcs from $F^H(\sigma_H)$ bounding C_i
- $L^i(\sigma_H)$ the set of ovals from $L^H(\sigma_H)$ bounding C_i .

Requirement for intersection points

An intersection point associated to a component C_i is given by a choice of $2m_i$ points on the punctured surface $(z_1^i, \dots, z_{m_i}^i)$ such that:

- (1) each arc from $F^i(\sigma_H)$ contains exactly one component $\{z_1^i, \dots, z_{m_i}^i\}$
- (2) each oval from $L^i(\sigma_H)$ contains one component from $\{z_1^i, \dots, z_{m_i}^i\}$.

We have the set of special points, that belong to our collections of arcs and ovals, which have the property that they very close to the base points. We denote them by:

$$(\bar{b}_1^i, \dots, \bar{b}_{m_i}^i).$$

When we following the open contour of our state circle, these points are chosen at intervals at Step 2, so

$$\bar{B}^i = (\bar{b}_1^i, \dots, \bar{b}_{m_i}^i)$$

provides a well defined intersection point that satisfies the above **Requirement for intersection points**.

Now, we investigate if it is possible to have other intersection points satisfying this requirement. We look at the arc containing \bar{b}_1^i . This arc intersects **just one oval**: the one containing \bar{b}_1^i . This is thanks to our choice of making the oval containing the base point b_m smaller, so this does not intersect this arc. So we are obliged to choose for this arc the point \bar{b}_1^i . Now, we look at the next arc. We are obliged to choose on it the point \bar{b}_1^i . Otherwise, we have in our collection of points two components on the same oval, which is not permitted. Inductively, we have to choose the last component to be $\bar{b}_{m_i}^i$. Overall, we see that we have exactly one intersection point: $\bar{B}^i = (\bar{b}_1^i, \dots, \bar{b}_{m_i}^i)$. □

Step 4- Computing the contribution of the loop associated to the cut state circle

We compute the contribution of the intersection point \bar{B}^i once we evaluate the local system and specialize it through $\alpha_Q^{\sigma_H}$. For this, we have to see which loop is associated to this intersection point.

If we have chosen the components of \bar{B}^i , then the loop associated to it starts in the base points

$$b_1^i, \dots, b_{m_i}^i,$$

continue by the connecting paths to the components

$$\bar{b}_1^i, \dots, \bar{b}_{m_i}^i,$$

then go back to the base points following a very little part of the ovals. We remark that this loop does not wind around any puncture, so the contribution of the intersection point \bar{B}^i to the local system gets evaluated to 1.

Step 5- Sign contribution of intersection point from the cut state circle

For the point \bar{B}^i we have all intersections between arcs and ovals with positive local orientations and also there is no permutation induced at the level of the set of arcs and ovals. So this point has a sign contribution of

$$+1.$$

Step 6- Contribution of intersection point associated to the cut circle to the intersection form

Overall we see that \bar{B}^i contributes to the local system evaluation by 1 and carries the sign 1.

This shows that the component C_i contributes to the intersection by 1. In particular, the **cut circle** does not contribute to the count of the local system, and it do not add any contribution. For all state circles, and we have $|\sigma_H - 1|$ of them, we obtain a contribution of $(1 - C)$. So, our intersection is indeed:

$$(47) \quad \ll \mathcal{F}^H(\sigma_H), \mathcal{L}^H(\sigma_H) \gg_{\alpha_Q^{\sigma_H}} = (1 - Q)^{|\sigma_H - 1|}.$$

which concludes the proof of the Lemma. □

Now we are ready to show that the above topological viewpoint, provided by the set of graded intersections of homology classes which are associated to the cut state circles give the HOMFLY-PT polynomial.

For the case of the HOMFLY-PT polynomial, we have introduced another specialization of coefficients, following Definition 3.23, as below:

$$(48) \quad \alpha_H^{\sigma_H} : \mathbb{Z}[x_1^{\pm 1}, \dots, x_{8n}^{\pm 1}] \rightarrow \mathbb{Z}[a^{\pm 1}, z^{\pm 1}](1 - \frac{a - a^{-1}}{z})$$

This has the associated specialized intersection pairing given by:

$$(49) \quad \ll , \gg_{\alpha_H^{\sigma_H}} : \mathcal{H}_{2n}^{lf} |_{\alpha_H^{\sigma_H}} \otimes \mathcal{H}_{2n} |_{\alpha_H^{\sigma_H}} \rightarrow \mathbb{Z}[a^{\pm 1}, z^{\pm 1}](1 - \frac{a - a^{-1}}{z}).$$

Lemma 5.11 (Recovering the HOMFLY-PT polynomial for un-links via arcs and ovals). *Let us fix a state $\sigma = \sigma_H$. Then, the intersection between the classes $\mathcal{F}^H(\sigma_H)$ and $\mathcal{L}^H(\sigma_H)$ specialized through α_H gives precisely the HOMFLY-PT bracket evaluated on the state circles associated to σ_H :*

$$(50) \quad \ll \mathcal{F}^H(\sigma_H), \mathcal{L}^H(\sigma_H) \gg_{\alpha_H^{\sigma_H}} = \left(\frac{a - a^{-1}}{z}\right)^{|\sigma_H^{-1}|}.$$

Proof. Following Lemma 4.6, we have that:

$$(51) \quad \ll \mathcal{F}^H(\sigma_H), \mathcal{L}^H(\sigma_H) \gg_{\alpha_Q^{\sigma_H}} = (1 - Q)^{|\sigma_H^{-1}|}.$$

In our case we have $Q = Q_H = 1 - \frac{a - a^{-1}}{z}$ and so this leads to our desired formula for the intersection:

$$(52) \quad \ll \mathcal{F}^H(\sigma_H), \mathcal{L}^H(\sigma_H) \gg_{\alpha_H^{\sigma_H}} = \left(\frac{a - a^{-1}}{z}\right)^{|\sigma_H^{-1}|}.$$

□

5.5. A topological model for the HOMFLY-PT polynomial. We use the state sum formulation (44) defined in the previous section to define Θ_H incorporating the intersection pairing that recovers the polynomial.

For a state σ_H We also define the monomial coefficients $i^a(\sigma_H), i^z(\sigma_H)$, summing over all local contributions.

- if χ is a positive crossing, then

$$(i_\chi^a(\sigma_H), i_\chi^z(\sigma_H)) := \begin{cases} (-1, 1) & \text{if } \sigma_H(\chi) = o \\ (-2, 0) & \text{if } \sigma'_H(\chi) = -\chi \end{cases}$$

- if χ is a negative crossing, then

$$(i_\chi^a(\sigma_H), i_\chi^z(\sigma_H)) := \begin{cases} (1, 1) & \text{if } \sigma(\chi) = o \\ (2, 0) & \text{if } \sigma \text{ chooses } -\chi \text{ at the crossing } \chi \end{cases}$$

Now let

$$i^a(\sigma_H) := \prod_{\chi \in c(D)} i_\chi^a(\sigma_H) \quad \text{and} \quad i^z(\sigma_H) := \prod_{\chi \in c(D)} i_\chi^z(\sigma_H),$$

with

$$\text{sgn}(\sigma_H) = \prod_{\chi \in c(D)} \text{sgn}(\chi).$$

Let $D_{\sigma_H}^a$ be a set of curves on Σ twisted by the oriented Kauffman state σ_o which gives boundary of the Seifert surface, with a modification that we put in additional twistings for those crossings of D on which $\sigma'(H)$ chooses $-\chi$.

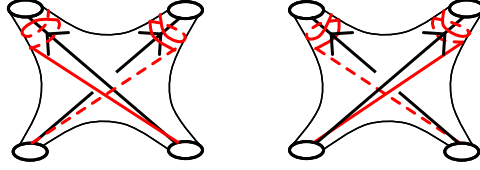


FIGURE 18.

The curves $D_{\sigma_H}^z$ will be twisted by the Kauffman state σ identical to σ_H , see Figure 12, with an adjustment to roll the twisting the other way for a negative crossing.

The functions $i^a(\sigma_H), i^z(\sigma_H)$ can similarly be defined as the geometric intersection of $D_{\sigma_H}^a$ and $D_{\sigma_H}^z$ with the link diagram D .

Lemma 5.12. *We have*

$$i^a(\sigma_H) = \frac{i(D_{\sigma_H}^a(\alpha), D)}{2}$$

$$i^z(\sigma_H) = \frac{i(D_{\sigma_H}^z(\alpha), D)}{2}$$

Proof. The intersection with the boundary of the Seifert surface for L constructed from D given by $\frac{i(D_{\sigma_H}^a(\alpha), D)}{2}$ will count -1 for a positive crossing χ on which $\sigma_H(\chi) = o$, and -2 for a positive crossing on which $\sigma_H(\chi) = -\chi$, due to the extra twistings that are placed for this case. The evaluation on a negative crossing is similar except for the opposite sign. For $i^z(\sigma_H)$, the intersection $\frac{i(D_{\sigma_H}^z(\alpha), D)}{2}$ will count 1 the crossings on which σ_H chooses the oriented resolution, and 0 for the crossings on which σ_H chooses the un-oriented resolution. \square

Finally, we obtain

(53)

$$P_L(a, z) = \sum_{\sigma_H \text{ a state on the diagram } D} \text{sgn}(\sigma_H) a^{i^a(\sigma_H)} z^{i^z(\sigma_H)} \left(\frac{a - a^{-1}}{z} \right)^{|\sigma_H| - 1}$$

where $|\sigma_H|$ is the number of circles in the set of circles resulting from applying the state σ_H to every crossing in the diagram D .

Now we are ready to prove Theorem 1.

5.6. Proof of Theorem 1. Let $i^a(\sigma_H), i^z(\sigma_H)$, and $\text{sgn}(\sigma_H)$ be defined as in the previous section, Section 5.5, and recall $\ll, \gg_{\alpha_H^{\sigma_H}}$ is the intersection pairing defined in Section 5.4.

Similarly to Θ_J , we define $\Theta_H(D)$:

Definition 5.13 (Intersection form for the HOMFLY-PT polynomial).

$$\Theta_H(D) := \sum_{\sigma_H \text{ a state on the diagram } D} \text{sgn}(\sigma_H) a^{i^a(\sigma_H)} z^{i^z(\sigma_H)} \ll F^H(\sigma), L^H(\sigma)_H \gg$$

We restate Theorem 1 for the convenience of the reader.

Theorem 5.14 (Theorem 1) (Topological model for the HOMFLY-PT polynomial via ovals).

Let $\Theta_H(D) \in \mathbb{Z}[a^{\pm 1}, z^{\pm 1}]$ be state sum of graded intersection between explicit Lagrangian submanifolds in a fixed configuration space on the Heegaard surface, as in Definition 1.5. Then this topological model recovers the HOMFLY-PT invariant:

$$\Theta_H(D) = P_L(a, z)$$

Proof. Since $\ll, \gg_{\alpha_H^{\sigma_H}}$ recovers $\left(\frac{a-a^{-1}}{z}\right)^{|\sigma_H|-1}$ in (53) by Lemma 5.11, it follows that $\Theta_H(D) = P_L(a, z)$. \square

REFERENCES

- [1] Cristina Ana-Maria Anghel. A globalisation of Jones and Alexander polynomials constructed from a graded intersection of two Lagrangians in a configuration space. ArXiv:2205.07842, 2022.
- [2] Cristina Ana-Maria Anghel. A topological model for the coloured Jones polynomials. *Selecta Math. (N.S.)*, 28(3):Paper No. 63, 50, 2022.
- [3] Cristina Ana-Maria Anghel. $U_q(sl(2))$ -quantum invariants from an intersection of two Lagrangians in a symmetric power of a surface. *Trans. Amer. Math. Soc.*, 376(10):7139–7185, 2023.
- [4] Cristina Ana-Maria Anghel. Witten-Reshetikhin-Turaev invariants for 3-manifolds from Lagrangian intersections in configuration spaces. *Quantum Topol.*, 14(4):693–731, 2023.
- [5] Cristina Ana-Maria Anghel and Martin Palmer. Lawrence-Bigelow representations, bases and duality, 2020. ArXiv:2011.02388.
- [6] Stephen Bigelow. A homological definition of the Jones polynomial. In *Invariants of knots and 3-manifolds (Kyoto, 2001)*, volume 4 of *Geom. Topol. Monogr.*, pages 29–41. Geom. Topol. Publ., Coventry, 2002.
- [7] Stephen Bigelow. A homological definition of the HOMFLY polynomial. *Algebr. Geom. Topol.*, 7:1409–1440, 2007.
- [8] Sergei Chmutov and Michael Polyak. Elementary combinatorics of the HOMFLYPT polynomial. *Int. Math. Res. Not. IMRN*, (3):480–495, 2010.
- [9] Oliver T. Dasbach, David Futer, Efstratia Kalfagianni, Xiao-Song Lin, and Neal W. Stoltzfus. The Jones polynomial and graphs on surfaces. *J. Combin. Theory Ser. B*, 98(2):384–399, 2008.
- [10] David Futer, Efstratia Kalfagianni, and Jessica S. Purcell. Slopes and colored Jones polynomials of adequate knots. *Proc. Amer. Math. Soc.*, 139(5):1889–1896, 2011.
- [11] Jim Hoste. A polynomial invariant of knots and links. *Pacific J. Math.*, 124(2):295–320, 1986.
- [12] François Jaeger. A combinatorial model for the Homfly polynomial. *European J. Combin.*, 11(6):549–558, 1990.
- [13] R. J. Lawrence. A functorial approach to the one-variable Jones polynomial. *J. Differential Geom.*, 37(3):689–710, 1993.
- [14] W. B. Raymond Lickorish. *An introduction to knot theory*, volume 175 of *Graduate Texts in Mathematics*. Springer-Verlag, New York, 1997.
- [15] Yoav Moriah. Heegaard splittings of knot exteriors. In *Workshop on Heegaard Splittings*, volume 12 of *Geom. Topol. Monogr.*, pages 191–232. Geom. Topol. Publ., Coventry, 2007.

- [16] Kunio Murasugi and Józef H. Przytycki. The skein polynomial of a planar star product of two links. *Math. Proc. Cambridge Philos. Soc.*, 106(2):273–276, 1989.
- [17] Peter Ozsváth and Zoltán Szabó. Heegaard Floer homology and alternating knots. *Geom. Topol.*, 7:225–254, 2003.
- [18] Józef H. Przytycki. Skein modules of 3-manifolds. *Bull. Polish Acad. Sci. Math.*, 39(1-2):91–100, 1991.

SCHOOL OF MATHEMATICS, UNIVERSITY OF LEEDS, WOODHOUSE, LEEDS LS2 9JT,
UNITED KINGDOM; INSTITUTE OF MATHEMATICS SIMION STOILOW OF THE ROMANIAN
ACADEMY, 21 CALEA GRIVITEI STREET, 010702 BUCHAREST, ROMANIA.

Email address: `c.a.palmer-anghel@leeds.ac.uk`, `cranghel@imar.ro`

TEXAS STATE UNIVERSITY, DEPARTMENT OF MATHEMATICS, SAN MARCOS, TX

Email address: `vne11@txstate.edu`